

Controlling unconventional superconductivity in artificially engineered f -electron Kondo superlattices

M. Naritsuka*, T. Terashima, and Y. Matsuda

Department of Physics, Kyoto University, Kyoto 606-8502 Japan

Unconventional superconductivity and magnetism are intertwined on a microscopic level in a wide class of materials, including high- T_c cuprates, iron pnictides, and heavy-fermion compounds. A new approach to this most fundamental and hotly debated subject focuses on the role of interactions between superconducting electrons and bosonic fluctuations at the interface between adjacent layers in heterostructures. A recent state-of-the-art molecular-beam-epitaxy technique has enabled us to fabricate superlattices consisting of different heavy-fermion compounds with atomic thickness. These Kondo superlattices provide a unique opportunity to study the mutual interaction between unconventional superconductivity and magnetic order through the atomic interface. Here, we design and fabricate hybrid Kondo superlattices consisting of alternating layers of superconducting CeCoIn₅ with d -wave pairing symmetry and nonmagnetic metal YbCoIn₅ or antiferromagnetic heavy fermion metals, such as CeRhIn₅ and CeIn₃. In these Kondo superlattices, superconducting heavy electrons are confined within the two-dimensional CeCoIn₅ block layers and interact with the neighboring nonmagnetic or magnetic layers through the interface. In CeCoIn₅/YbCoIn₅ superlattices, the superconductivity is strongly influenced by the local inversion symmetry breaking at the interface. In CeCoIn₅/CeRhIn₅ and CeCoIn₅/CeIn₃ superlattices, the superconducting and antiferromagnetic states coexist in spatially separated layers, but their mutual coupling via the interface significantly modifies the superconducting and magnetic properties. The fabrication of a wide variety of hybrid superlattices paves a new way to study the relationship between unconventional superconductivity and magnetism in strongly correlated materials.

I. INTRODUCTION

Superconductivity found in several classes of strongly correlated electron systems, including cuprates[1, 2], iron pnictides/chalcogenides[3–5] and heavy fermion compounds[6, 7] has attracted researchers over the past three decades. There is almost complete consensus that superconductivity in these systems cannot be explained by the conventional electron-phonon attractive pairing interactions [8, 9]. As the superconductivity occurs in the vicinity of the magnetic order, it is widely believed that magnetic fluctuations, which arises from purely repulsive Coulomb interactions, act as the source of electron pairing. Moreover, the highest superconducting transition temperature T_c is often found near a quantum critical point (QCP), at which a magnetic phase vanishes in the limit of zero temperature, indicating that proliferation of critical magnetic excitations resulting from the QCP plays a significant role in determining superconducting properties [10–16]. In these materials, a microscopic coexistence of superconducting and magnetically ordered phases both involving the same charge carriers is a striking example of unusual emergent electronic phases. Despite tremendous research, however, the relationship between superconductivity and magnetism has remained largely elusive.

The strongest electron correlation is realized in heavy-fermion compounds, containing f electrons ($4f$ for lan-

thanide and $5f$ for actinide), especially in materials containing Ce, Pr, U and Pu atoms [17–23]. At high temperature, f electrons are essentially localized with well-defined magnetic moments. As the temperature is lowered, the f electrons begin to delocalize due to the hybridization with conduction electron band (s , p , d orbital), and Kondo screening. At yet lower temperature, the f electrons become itinerant, forming a narrow conduction band with heavy effective electron mass (up to a few hundred to a thousand times the free electron mass). Strong Coulomb repulsion within a narrow band and the magnetic interaction between remnant unscreened $4f$ or $5f$ moments leads to notable many-body effects, and superconductivity mediated by magnetic fluctuations. The hybridized f electrons are not only responsible for long-range magnetic order, but are also involved in superconductivity. Therefore, the heavy-fermion compounds offer a fascinating playground where magnetism and unconventional superconductivity can both compete and coexist.

Among heavy fermion compounds, Ce M In₅ (where M = Co, and Rh) with layered structure are ideal model systems due to their rich electronic phase diagrams in which an intricate interplay between superconductivity and magnetism is observed [24–26]. At ambient pressure, CeCoIn₅ is a superconductor ($T_c = 2.3$ K) with $d_{x^2-y^2}$ -wave symmetry [27–31]. The normal state displays non-Fermi-liquid properties associated with a nearby underlying QCP [32, 33]. In contrast, CeRhIn₅ orders antiferromagnetically at ambient pressure ($T_N = 3.8$ K) [34]. Its magnetic transition is suppressed by applying pressure and the ground state becomes a purely superconducting state at $P > P \approx 1.7$ GPa, suggesting a possible presence

*Present address: School of Physics and Astronomy, University of St Andrews, North Haugh, St Andrews, Fife KY16 9SS, UK.

of a pressure-induced QCP [11, 13, 35–39].

It has been shown that interactions between superconducting electrons and bosonic excitations through an atomic interface may have a profound influence on Cooper pairing. For example, when a monolayer FeSe film grown on a SrTiO₃ substrate, the coupling between the FeSe electrons and SrTiO₃ phonons enhances the Cooper pairing, giving rise to the highest T_c among all known iron-based superconductor, which is almost an order of magnitude higher than that of the bulk FeSe [5, 40–43]. This raises the possibility of a magnetic analog in which the pairing interaction is influenced by magnetic fluctuations through an interface between an unconventional superconductor and a magnetic metal. This concept is illustrated schematically in Figs. 1(a) and 1(b). Besides allowing a new approach to revealing the entangled relationship between magnetism and unconventional superconductivity, this concept has the advantage that magnetic excitations are tunable as a magnetic transition is driven toward zero temperature, unlike phonon excitations in SrTiO₃.

In this review, we discuss the recent advances of Kondo superlattices which consist of alternating layers of heavy-fermion superconductor and heavy-fermion antiferromagnet. We focus on mutual interactions between d -wave superconductivity and magnetic order through the atomic interface, in particular paying attention to how the pairing interaction is influenced by magnetic fluctuations injected from the neighboring layers through the atomic interface. For this purpose, we have designed and fabricated two types of superlattices formed by alternating atomically thick layers of CeCoIn₅ and (1) conventional non-magnetic metal YbCoIn₅ and (2) antiferromagnetic (AFM) heavy fermion metals, such as CeRhIn₅ and CeIn₃. In these Kondo superlattices, superconducting heavy electrons are confined within the two-dimensional (2D) CeCoIn₅ block-layers (BLs) and interact with the neighboring nonmagnetic or magnetic layers through the interface. In CeCoIn₅/YbCoIn₅ superlattices, local inversion symmetry breaking at the interface enables Rashba spin-orbit coupling to play a key role in superconductivity [44–47]. In CeCoIn₅/CeRhIn₅ and CeCoIn₅/CeIn₃ Kondo superlattices, the superconducting and AFM states coexist in spatially separated layers [48, 49]. The AFM ordering temperature of CeRhIn₅ and CeIn₃ BLs can be tuned to zero by applying hydrostatic pressure, leading to a magnetic QCP. In these superlattices, we show that the superconducting and non-

superconducting magnetic layers can interact with each other. In particular, in CeCoIn₅/CeRhIn₅ superlattices, upon suppressing the AFM order, the force binding superconducting electron pairs acquires an extreme strong coupling nature superlattices, demonstrating that superconducting pairing can be tuned nontrivially by magnetic fluctuations injected through the interface.

II. KONDO SUPERLATTICE

A. Kondo superlattice

Recently, the state-of-the-art molecular beam epitaxy (MBE) technique enables the realization of high quality hetero-interface of heavy fermion systems through the fabrication of Ce-based compounds [44, 50, 51]. Superlattices consisting of alternating layers of superconductor CeCoIn₅, nonmagnetic metals, such as YbCoIn₅ and YbRhIn₅, and AFM heavy fermion metals, such as CeRhIn₅ and CeIn₃ [48, 49] with atomic layer thicknesses have been fabricated.

Here we design and fabricate three kinds of superlattices formed by alternating atomically thick layers of CeCoIn₅ and (1)YbCoIn₅, (2)CeRhIn₅ and (3)CeIn₃. YbCoIn₅ and Ce M In₅ ($M = \text{Co}$ and Rh) crystalize in the tetragonal HoCoGa₅ structure. Ce M In₅ can be viewed as alternating layers of CeIn₃ and M In₂ stacked sequentially along the tetragonal c -axis. CeIn₃ has a cubic AuCu₃-type structure with a 3D Fermi surface. It should be noted that as disorder may greatly influence physical properties, especially near a QCP, there is a great benefit in examining quantum critical systems that are stoichiometric and hence relatively disorder free; these heavy fermion compounds are examples of a small number of such systems.

B. Layered heavy-fermion CeCoIn₅ and CeRhIn₅

CeCoIn₅ is a heavy-fermion superconductor with $T_c = 2.3$ K, which is the highest among Ce-based heavy-fermion superconductors [52]. Related to the layered structure, de Haas–van Alphen experiments on CeCoIn₅ reveal a corrugated cylindrical Fermi surface [52, 53]. In addition, nuclear magnetic resonance (NMR) relaxation rate T_1 measurements indicate the presence of anisotropic (quasi-2D) AFM spin fluctuations in the normal state [54, 55]. A large Sommerfeld constant $\gamma = C/T = 290$ mJ mol⁻¹K⁻² is observed just above T_c [56]. The normalized jump in heat capacity $\Delta C/\gamma T_c \sim 4.5$ suggests that CeCoIn₅ exhibits very strong coupling superconductivity compared with the BCS value of 1.43 [57]. The normal state possesses non-Fermi-liquid properties in zero fields, including T -linear resistivity, indicating a nearby underlying QCP [32, 58]. It is well established by several experiments that the superconducting gap has $d_{x^2-y^2}$ -wave symmetry, which is a strong indication for magnet-

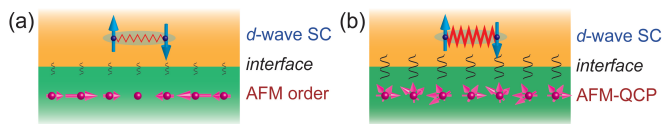


FIG. 1: (a) Schematic figure of the interaction between d -wave superconducting (SC) state and static AFM order via the interface. (b) Interaction between two competing orders under pressure near a QCP, where AFM order disappears.

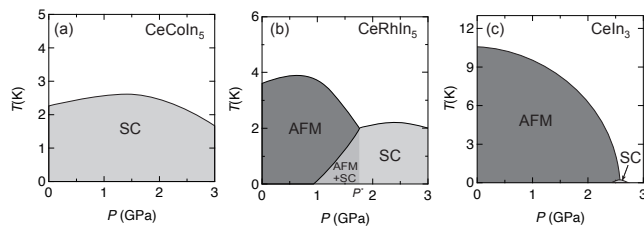


FIG. 2: Schematic pressure-temperature phase diagrams of (a) CeCoIn₅, (b) CeRhIn₅, and (c) CeIn₃. Regions of antiferromagnetic order and superconducting state are indicated by AFM and SC, respectively.

ically mediated Cooper pairing [27–31]. Inelastic neutron scattering measurements detected the presence of magnetic fluctuations at the incommensurate wavevector $q = (0.45, 0.45, 0.5)$ [59].

The magnetic field destroys the superconductivity in two distinct ways, the orbital pair-breaking effect (vortex formation) and the Pauli paramagnetic effect, a breaking up of pairs by spin polarization. In CeCoIn₅, the upper critical field H_{c2} for both $\mathbf{H} \parallel ab$ and $\mathbf{H} \perp ab$ is limited by extremely strong Pauli pair-breaking [13, 27, 60]. The Pauli-limited upper critical field H_{c2}^{Pauli} is given by [61]

$$H_{c2}^{\text{Pauli}} = \sqrt{2}\Delta/g\mu_B, \quad (1)$$

where g is the gyromagnetic ratio, which is determined by the Ce crystalline electric field levels for CeCoIn₅, and Δ is the superconducting gap energy. As a result of strong Pauli effect on the superconductivity, a possible Fulde–Ferrel–Larkin–Ovchinnikov state has been suggested [25, 62–67].

At ambient pressure, superconductivity in CeCoIn₅ emerges from a non-Fermi liquid state. The normal state resistivity shows a linear temperature dependence, $\rho(T) \propto T$ over a wide temperature range [32]. The electronic heat capacity in magnetic field, which is enough to suppress the superconductivity, exhibits a logarithmic increase, $C_e(T)/T \propto -\ln T$ [52]. These have been discussed in terms of the hallmarks of non-Fermi liquid behavior near the 2D AFM QCP [68]. With apply pressure, the Fermi liquid behavior is recovered in resistivity and heat capacity [52, 57, 69]. The pressure-temperature (P – T) phase diagram is displayed in Fig. 2(a).

CeRhIn₅ has a smaller quasi-2D Fermi surface than that of CeCoIn₅ with reflecting localized nature of f -electrons. At ambient pressure, CeRhIn₅ undergoes an AFM transition at Néel temperature $T_N = 3.8$ K, with the ordered magnetic moment of $0.75 \mu_B$, and with an incommensurate wave vector $\mathbf{q} = (0.5, 0.5, 0.297)$ helical in the c -axis direction [34]. The ¹¹⁵In nuclear quadrupole resonance (NQR) measurements suggested that in the ordered state the magnetic moments lie strictly in the CeIn₃ plane and a spiral spin structure is realized along the c -axis direction [70]. With increasing pressure P , T_N increases and shows a maximum at $P \sim 1$ GPa where

superconductivity appears [11]. At higher pressures, the AFM phase and the superconducting phase coexist, and T_c increases with pressure but T_N decreases [71]. Above the pressure P^* where $T_c = T_N$, the AFM order suddenly disappears and the pressure-induced transition to superconductivity appears to be first order, thus avoiding a QCP. Apparent deviations from Fermi liquid behavior have been observed in $\rho(T)$ over a wide temperature and pressure range [37]. The P – T phase diagram is displayed in Fig. 2(b).

C. Antiferromagnetic heavy fermion CeIn₃

At ambient pressure, CeIn₃ undergoes an AFM transition at $T_N = 10.1$ K with an ordered magnetic moment of $0.48 \mu_B$ and a commensurate wave vector $\mathbf{q} = (0.5, 0.5, 0.5)$ [72, 73]. A dome-like superconducting phase appears with $T_c^{\text{max}} = 0.2$ K around the critical pressure $P_c = 2.6$ GPa, which indicates that the superconductivity is believed to be mediated by quantum critical spin fluctuations [10, 73]. The normal state resistivity near the critical pressure shows non-Fermi liquid behavior [74], $\rho(T) \sim T^\alpha$ with $\alpha = 1.6$, which strongly deviate from the Fermi liquid value of $\alpha = 2$. This critical exponent α near P_c is close to $3/2$ reflecting 3D AFM magnetic fluctuations [75], indicating the existence of 3D AFM QCP. The P – T phase diagram is displayed in Fig. 2(c).

D. Non-magnetic metal YbCoIn₅

The Yb-ions in YbCoIn₅ are divalent and form the closed-shell $4f$ configuration [76]. As a result, YbCoIn₅ is a nonmagnetic compound, showing conventional metallic behavior in resistivity and magnetic susceptibility [77]. No superconducting transition has been reported in bulk and thin film YbCoIn₅ at ambient and under pressure [48, 77].

III. EXPERIMENTAL METHOD

A. Molecular beam epitaxy systems

MBE is essentially a refined ultra-high-vacuum evaporation method, which helps to prevent contamination of the surface and oxidation of elements such as Ce. Thus, high-quality thin films of Ce based compounds can be grown using MBE. MBE enables a slow growth rate of 0.01–0.02 nm/s that permits very precise control of layer thickness. Consequently, abrupt material interfaces can be achieved, enabling the fabrication of heterostructures such as superlattices. The typical pressure in the MBE chamber is maintained at $< 10^{-7}$ Pa during the fabrication of thin films, enabling powerful diagnostic techniques such as reflection high-energy electron diffraction

(RHEED) for *in situ* monitoring of thin films' growth without the complication of surface degradation.

Magnesium fluoride MgF_2 is used as the substrate. MgF_2 has a rutile-type tetragonal structure with a lattice parameter $a = 0.462$ nm, which matches the lattice parameters $a = 0.468, 0.453, 0.461$ and 0.465 nm for CeIn_3 , YbCoIn_5 , CeCoIn_5 and CeRhIn_5 , respectively. Furthermore, because MgF_2 does not contain oxygen, the oxidation of Ce compounds during the growth can be avoided. Thus, single-crystal MgF_2 is a suitable substrate material to support the epitaxial growth of CeIn_3 and CeCoIn_5 thin films. To relax the lattice mismatch and improve the quality of the superlattice, we first grow buffer layers. Initially, 30 nm of CeIn_3 buffer layers were grown at 450°C . Subsequently, 15 nm of YbCoIn_5 buffer layers were grown at 550°C . On top of these, superlattice layers were grown. For $\text{CeCoIn}_5/\text{CeIn}_3$ superlattices, ~ 5 nm of the cobalt is deposited as a capping layer at room temperature to avoid the oxidization of samples.

In what follows, we denote a superlattice with alternating layers of n -UCT CeCoIn_5 and m -UCT CeRhIn_5 as $\text{CeCoIn}_5(n)/\text{CeRhIn}_5(m)$.

The left panel of Fig. 3 displays high-resolution cross-sectional transmission electron microscope (TEM) image of $\text{CeCoIn}_5(1)/\text{YbCoIn}_5(5)$ superlattice, where 1-UCT CeCoIn_5 layer are sandwiched by 5-UCT YbCoIn_5 layers. The bright dot arrays are identified as the Ce layers and the less bright dots are Yb atoms, which is consistent with the designed superlattice structure. As shown in the right panel of Fig. 3, the intensity integrated over the horizontal width of the image plotted against the vertical position indicates a clear difference between the Ce and Yb layers, showing no discernible atomic interdiffusion between the neighboring Ce and Yb layers.

Figures 4(a) and 4(b) display high resolution cross-sectional TEM images of $\text{CeCoIn}_5(5)/\text{CeRhIn}_5(5)$ and $\text{CeCoIn}_5(7)/\text{CeIn}_3(13)$ superlattices, respectively. A clear interface between CeCoIn_5 and CeRhIn_5 or CeIn_3 layers is observed. Figures 4(c) and 4(d) display electron energy loss spectroscopy (EELS) images of $\text{CeCoIn}_5(5)/\text{CeRhIn}_5(5)$ and $\text{CeCoIn}_5(7)/\text{CeIn}_3(13)$ su-

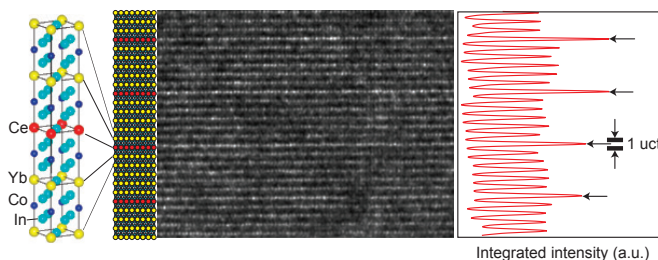


FIG. 3: Cross-sectional TEM image of the $\text{CeCoIn}_5(1)/\text{YbCoIn}_5(5)$ superlattice. The bright dot arrays are identified as the Ce layers and the less bright dots are Yb atoms. The right panel represents the intensity integrated over the horizontal width of the TEM image plotted against the vertical position.

perlattices, respectively. The EELS images clearly resolve CeCoIn_5 , CeRhIn_5 or CeIn_3 BLs, demonstrating sharp interfaces with no atomic interdiffusion between the neighboring BLs.

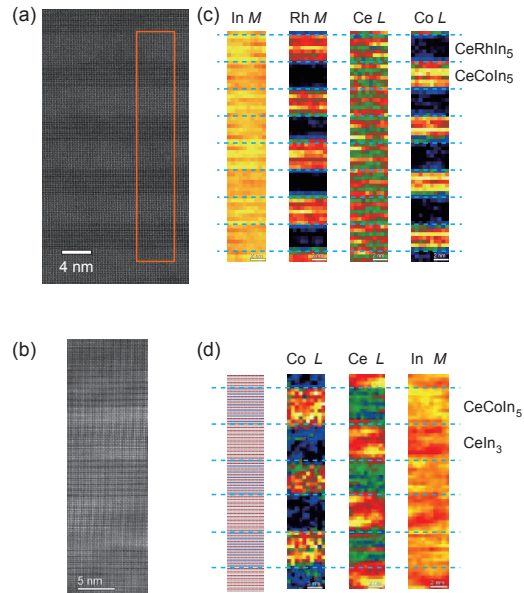


FIG. 4: (a) and (b) represent high-resolution cross-sectional TEM and images for $\text{CeCoIn}_5(5)/\text{CeRhIn}_5(5)$ and $\text{CeCoIn}_5(7)/\text{CeIn}_3(13)$ superlattices, respectively. (c) EELS images measured in the boxed area in the TEM image of (a) for In M , Rh M , Ce L , and Co L edges. (d) EELS image for the $\text{CeCoIn}_5(7)/\text{CeIn}_3(13)$ superlattice with the electron beam aligned along the (100) direction. The EELS images were taken for Co L , Ce L , and In M edges.

For all the above Kondo superlattices, streak patterns of the RHEED image were observed during the whole growth of the superlattices, indicating good epitaxy. In addition, the atomic-force-microscope measurements reveal that the surface roughness of both superlattices is within ± 1 nm, which is comparable to 1–2 UCT along the c axis of the constituents. Because atomically flat regions extend over distances of $\sim 0.1 \mu\text{m}$, it can be expected that transport properties are not seriously influenced by the roughness. Superlattice structures were also confirmed by the satellite peaks of the x-ray diffraction patterns for all superlattices. These results demonstrate the successful fabrication of epitaxial superlattices with sharp interfaces, revealing that the MBE technology is well suited for achieving our goal of designing Kondo superlattices.

B. Pressure experiments

In-plane resistivity measurements under pressure were performed with a commercial piston-cylinder-type high-pressure cell (CT Factory, Ltd.) [78]. We used Daphne7373 oil as the pressure medium. We applied

a load with a 20 tons hydraulic pressure machine at room temperature. The pressure inside the pressure cell was determined by the superconducting transition of lead (Pb), which was obtained by the quasi-four terminal resistivity measurement. A long and narrow shaped Pb installed inside the sample space is sensitive to the pressure gradient for the axial direction of the cell, which can be known by examining the width of the superconducting transition. In this study, the transition width was within 20 mK, indicating a good hydrostatic condition.

IV. HEAVY FERMION SUPERCONDUCTIVITY AT THE METALLIC INTERFACE

A. 2D confinement of heavy fermion superconductivity

In CeCoIn₅/YbCoIn₅ superlattices, the Ruderman-Kittel-Kasuya-Yosida (RKKY) interaction between the Ce atoms in neighboring CeCoIn₅ BLs is substantially reduced [79]. Moreover, the superconducting proximity effect between CeCoIn₅ and YbCoIn₅ layers is negligibly small due to the large Fermi velocity mismatch [80]. Then an important question is whether the superconducting electrons in the superlattices are heavy and if so what their dimensionality is. When the thickness of the CeCoIn₅ BL is comparable to the perpendicular coherence length ξ_c (about 2.1 nm for CeCoIn₅), and the separation of superconducting layers (~ 3.7 nm for CeCoIn₅(*n*)/YbCoIn₅(5) superlattices) exceeds ξ_c , each CeCoIn₅ BL acts as a 2D superconductor [44, 45, 81].

Figure 5(a) depicts the magnetic-field dependence of resistivity for CeCoIn₅(3)/YbCoIn₅(5) superlattice at several field angles from $\theta = 0$ ($\mathbf{H} \perp ab$) to 90 ($\mathbf{H} \parallel a$) at $T=150$ mK. Figure 5(b) shows the anisotropy of upper critical field $H_{c2\parallel}/H_{c2\perp}$, where $H_{c2\parallel}$ and $H_{c2\perp}$ are critical field parallel and perpendicular to the ab plane, as a function of reduced temperature T/T_c for CeCoIn₅(*n*)/YbCoIn₅(5) superlattices with $n=3, 5$ and 7 and for the bulk CeCoIn₅. H_{c2} is determined by the mid-point of the resistive transition. Unlike the almost T -independent anisotropy seen in single crystal of CeCoIn₅, anisotropy in the superlattice shows a divergent increase toward T_c . This diverging anisotropy is characteristic of 2D superconductivity, in which $H_{c2\parallel}$ increases as $\sqrt{T_c - T}$ due to the Pauli paramagnetic limiting, but $H_{c2\perp}$ increases as $T_c - T$ due to orbital limiting near T_c .

The 2D superconductivity is also confirmed from the angle variation of $H_{c2}(\theta)$ shown in Fig. 5(c). For 3D anisotropic mass model, $H_{c2}(\theta)$ is represented as [82]

$$H_{c2}(\theta) = H_{c2\parallel} / (\sin^2 \theta + \gamma_m^2 \cos^2 \theta)^{1/2}, \quad (2)$$

where $\gamma_m = H_{c2\parallel}/H_{c2\perp}$. In this model, H_{c2} varies smoothly with field orientation. We note that when H_{c2} is limited by Pauli paramagnetic effect as represented by Eq. (1), H_{c2} also varies smoothly as a function of θ . On

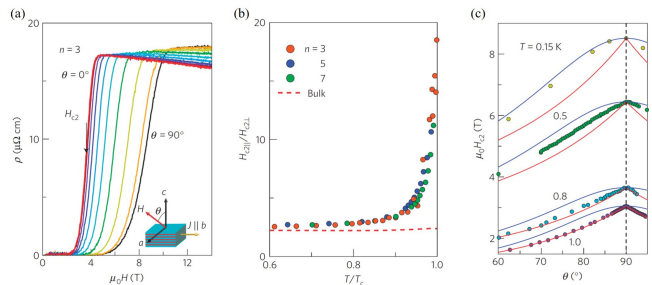


FIG. 5: (a) Field dependence of resistivity for CeCoIn₅(3)/YbCoIn₅(5) at several field angles from $\mathbf{H} \perp ab$ ($\theta = 0$) to $\mathbf{H} \parallel a$ ($\theta = 90$) at $T=150$ mK. (b) $H_{c2\parallel}/H_{c2\perp}$ vs. T/T_c , for the $n = 3, 5$, and 7 superlattices and for the bulk CeCoIn₅. (c) Angular dependence of the upper critical field, $H_{c2}(\theta)$. The blue and red lines represent fits to the data using the 3D anisotropic mass model (Eq.(2)) and the 2D Tinkham model (Eq.(3)), respectively.

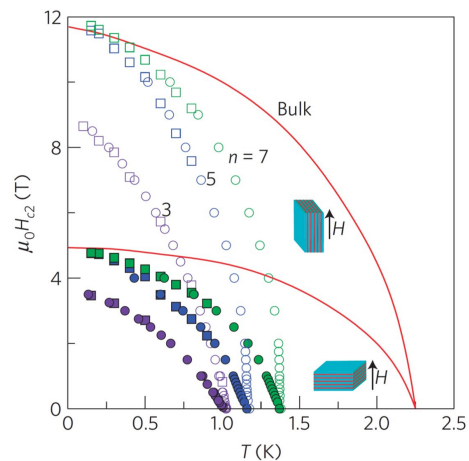


FIG. 6: H - T phase diagram of $n=3, 5$ and 7 superlattices in magnetic field parallel (open symbols) and perpendicular (closed symbols) to the ab plane, compared to the bulk CeCoIn₅ data.

the other hand, for 2D superconductor and Josephson coupled layered superconductors, $H_{c2}(\theta)$ is represented by Tinkham's formula as [83]

$$|H_{c2}(\theta) \cos \theta / H_{c2\perp}| + |H_{c2}(\theta) \sin \theta / H_{c2\parallel}|^2 = 1. \quad (3)$$

At $\theta = 90^\circ$, $H_{c2}(\theta)$ exhibits a sharp cusp. The solid blue and red lines in Fig. 5(c) are the fits to Eq. (2) and Eq. (3), respectively. A clear cusp at $\theta = 90^\circ$ is observed at $T=0.8$ and 1.0 K, indicating the 2D superconductivity. The cusp-like behavior of $H_{c2}(\theta)$ becomes less pronounced well below T_c , which is the opposite trend to the $H_{c2}(\theta)$ behavior of conventional multilayer systems. This suggests that $H_{c2}(\theta)$ at low temperatures is dominated by the Pauli effect in any field directions.

Figure 6 shows H - T phase diagram of CeCoIn₅(*n*)/YbCoIn₅(5) superlattices with $n=3, 5$ and 7 in magnetic field parallel (open symbols) and perpendicular (closed symbols) to the ab plane. For

the comparison, the results of the bulk CeCoIn₅ are also plotted. At low temperatures $H_{c2\parallel}$ and $H_{c2\perp}$ of the superlattices are significantly larger than those in conventional superconductors with similar T_c . The zero-temperature value of the orbital upper critical field in perpendicular field $H_{c2\perp}^{\text{orb}}(0)$ reflects the effective electron mass in the plane m_{ab}^* , $H_{c2\perp}^{\text{orb}}(0) \propto m_{ab}^{*2}$. Here, $H_{c2\perp}^{\text{orb}}(0)$ is determined from the initial slope of $H_{c2\perp}(T)$ at T_c through the relation [84],

$$H_{c2\perp}^{\text{orb}} \approx 0.69T_c(-dH_{c2\perp}/dT)_{T_c}. \quad (4)$$

$H_{c2\perp}^{\text{orb}}(0)$ is estimated to be 6, 11 and 12 T for CeCoIn₅(n)/YbCoIn₅(5) with $n=3, 5$ and 7, respectively. These magnitudes are comparable with or of the same order as $H_{c2\perp}^{\text{orb}}(0)$ (=14 T) in bulk CeCoIn₅ [44].

Based on these results, we conclude the 2D confinement of the superconducting ‘heavy’ electrons in the CeCoIn₅/YbCoIn₅ superlattices.

B. Local inversion symmetry breaking

In Fig. 7, $H_{c2\perp}$ normalized by $H_{c2\perp}^{\text{orb}}(0)$ for CeCoIn₅(n)/YbCo₅(5) superlattices with $n=3, 5$ and 7 is plotted as a function of the normalized temperature T/T_c . Two extreme cases, i.e., the result of the bulk single crystal of CeCoIn₅ dominated by Pauli paramagnetic effect and the Werthamer-Helfand-Hohenberg (WHH) curve with no Pauli effect [84], are also shown. For all superlattices, $H_{c2\perp}/H_{c2\perp}^{\text{orb}}(0)$ is much larger than that of single crystal CeCoIn₅, indicating that Pauli paramagnetic pair breaking effect is reduced in these superlattices. More importantly, $H_{c2\perp}/H_{c2\perp}^{\text{orb}}(0)$ is strikingly enhanced with decreasing n .

Recently, it has been suggested that the inversion symmetry breaking (ISB), together with strong spin-orbit interaction, can dramatically affect the superconductivity[85–87]. It has also been pointed out that such phenomena are more pronounced in strongly correlated electron systems. The inversion symmetry imposes important constraints on the pairing states: In the presence of inversion symmetry, Cooper pairs are classified into a spin-singlet or triplet state, whereas in the absence of inversion symmetry, an asymmetric potential gradient ∇V yields a spin-orbit interaction that breaks parity, and the admixture of spin-singlet and triplet states is possible. For instance, asymmetry of the potential in the direction perpendicular to the 2D plane $\nabla V \parallel [011]$ induces Rashba spin-orbit interaction

$$\alpha_R \mathbf{g}(\mathbf{k}) \cdot \boldsymbol{\sigma} \propto (\mathbf{k} \times \nabla V) \cdot \boldsymbol{\sigma}, \quad (5)$$

where $\mathbf{g} = (-k_y, k_x, 0)/k_F$, k_F is the Fermi wave number, and $\boldsymbol{\sigma}$ is the Pauli matrix. Rashba interaction splits the Fermi surface into two sheets with different spin structures [87–89]. The energy splitting is given by α_R , and the spin direction is tilted into the plane, rotating clockwise on one sheet and anticlockwise on the other. When

the Rashba splitting exceeds the superconducting gap energy ($\alpha_R > \Delta$), the superconducting properties are dramatically modified. As the spin-orbit interaction is generally significant in Ce-based superconductors, the introduction of ISB makes the systems a fertile ground for observing exotic properties. Moreover, theoretical studies suggest that when the interlayer hopping integral is comparable to, or smaller than, the Rashba splitting ($t_c \leq \alpha_R$), the local ISB plays an important role in determining the nature of the superconducting state[86]. This appears to be the case for the CeCoIn₅/YbCoIn₅ superlattices.

Although these superlattices maintain centrosymmetry, it has been suggested that the local ISB at the interface between two compounds influences the superconducting. Figure 8(a) represents the schematic representation of CeCoIn₅(m)/YbCoIn₅(5) superlattice. The middle CeCoIn₅ layer in a given CeCoIn₅ BL indicated by the gray plane is a mirror plane. The green (small) arrows represent the asymmetric potential gradient associated with the local ISB, $-\nabla V_{\text{local}}$. The Rashba splitting occurs at the interface between the CeCoIn₅ and YbCoIn₅ due to the local ISB. The spin direction is rotated in the ab plane and is opposite between the top and bottom CeCoIn₅ layers. Because the fraction of noncentrosymmetric interface layers increases with decreasing n , the observed remarkable enhancement of $H_{c2\perp}/H_{c2\perp}^{\text{orb}}(0)$ with decreasing n shown in Fig. 7 is attributed to the increased importance of the local ISB.

It has been reported that the local ISB also seriously

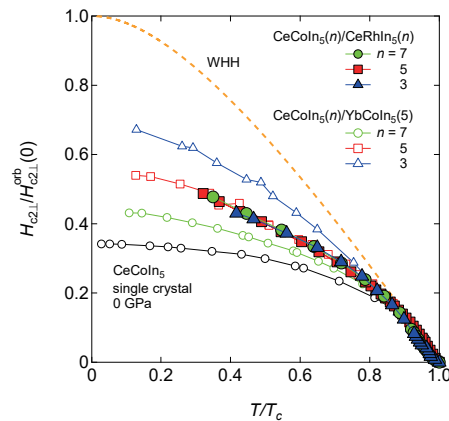


FIG. 7: Out-of-plane upper critical field $H_{c2\perp}$ normalized by the orbital-limited upper critical field at $T = 0$ K, $H_{c2\perp}/H_{c2\perp}^{\text{orb}}(0)$, for CeCoIn₅(n)/YbCoIn₅(5) and CeCoIn₅(n)/CeRhIn₅(n) superlattices with $n = 7, 5$, and 3 are plotted as a function of the normalized temperature T/T_c . Two extreme cases, i.e., the result of the bulk CeCoIn₅ dominated by Pauli paramagnetic effect and the WHH curve with no Pauli effect, are also shown. In CeCoIn₅(n)/YbCoIn₅(5), $H_{c2\perp}/H_{c2\perp}^{\text{orb}}(0)$ is enhanced with decreasing n , indicating the importance of the local ISB. In contrast, in CeCoIn₅(n)/CeRhIn₅(n), $H_{c2\perp}/H_{c2\perp}^{\text{orb}}(0)$ is independent of n .

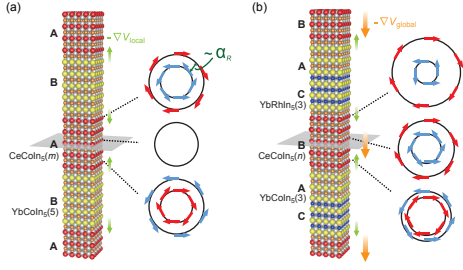


FIG. 8: (a) Schematic representation of bicolor Kondo superlattice $\text{CeCoIn}_5(m)/\text{YbCoIn}_5(5)$. The center of a CeCoIn_5 BL (ash plane) is a mirror plane. The green (small) arrows represent the asymmetric potential gradient associated with the local ISB, $-\nabla V_{\text{local}}$. The Rashba splitting occurs at the interface between the CeCoIn_5 and YbCoIn_5 BLs due to the local ISB. The spin direction is rotated in the ab plane and is opposite between the top and bottom CeCoIn_5 BLs. (b) Schematic representation of noncentrosymmetric tricolor Kondo superlattices $\text{YbCoIn}_5(3)/\text{CeCoIn}_5(n)/\text{YbRhIn}_5(3)$. The orange (large) arrows represent the asymmetric potential gradient $-\nabla V_{\text{global}}$. In the tricolor superlattices, all layers are not the mirror planes. The orange arrows represent the asymmetric potential gradient $-\nabla V_{\text{global}}$ due to the global broken inversion symmetry. The amplitude of Rashba splitting at the top layer of CeCoIn_5 BL is larger than that at the bottom of the BL, owing to the presence of $-\nabla V_{\text{global}}$ shown by the green small arrows.

influence the magnetic properties in non-superconducting Kondo superlattices. In $\text{CeRhIn}_5/\text{YbRhIn}_5$ superlattices, with reducing the thickness of magnetic CeRhIn_5 BLs, the Néel temperature is suppressed and the quasi-particle mass is strongly enhanced, implying dimensional control toward a magnetic QCP [90].

C. Tricolor Kondo superlattices

Recently, it has been reported that the magnitude of the Rashba spin-orbit interaction arising from the ISB is controllable by fabricating two types of Kondo superlattices[46, 91]. One is the introduction of the thickness modulation of YbCoIn_5 BLs that breaks the inversion symmetry centered at the superconducting block of CeCoIn_5 . The other is the ‘tricolor’ superlattices, in which CeCoIn_5 BLs are sandwiched by two different nonmagnetic metals, YbCoIn_5 and YbRhIn_5 , as illustrated in Fig. 8(b). In these two types of Kondo superlattices, the weakening of the Pauli paramagnetic pair breaking effect is more pronounced than that in ‘bicolor’ $\text{CeCoIn}_5/\text{YbCoIn}_5$ superlattices, as revealed by the further enhancement of $H_{c2\perp}/H_{c2\perp}^{\text{orb}}(0)$.

In particular, in the tricolor Kondo superlattices, the Rashba spin-orbit- interaction induced global inversion symmetry breaking is largely tunable by changing the layer thicknesses of YbCoIn_5 and YbRhIn_5 , leading to profound changes in the superconducting properties of 2D CeCoIn_5 BLs. Remarkably, the temperature depen-

dence of $H_{c2\parallel}$ of $\text{YbCoIn}_5(3)/\text{CeCoIn}_5(n)/\text{YbRhIn}_5(3)$, in which 3-UTC YbCoIn_5 , n -UCT CeCoIn_5 ($n = 5$ and 8) and 3-UCT YbRhIn_5 are stacked alternatively, in-plane upper critical field exhibits an anomalous upturn at low temperatures, which is attributed to a possible emergence of a helical or stripe superconducting phase [91]. These results demonstrate that the tricolor Kondo superlattices provide a new playground for exploring exotic superconducting states in the strongly correlated 2D electron systems with the Rashba effect.

The fabrication of tricolor superlattices containing d -wave superconducting layers offers the prospect of achieving even more fascinating pairing states than bulk CeCoIn_5 , such as helical and stripe superconducting states [92], a pair-density-wave state [93], complex stripe state [94], a topological crystalline superconductivity [95, 96], and Majorana fermion excitations[97–101], in strongly correlated electron systems.

V. TUNING THE PAIRING INTERACTION THROUGH THE INTERFACE

A. $\text{CeCoIn}_5/\text{CeRhIn}_5$ Kondo superlattices

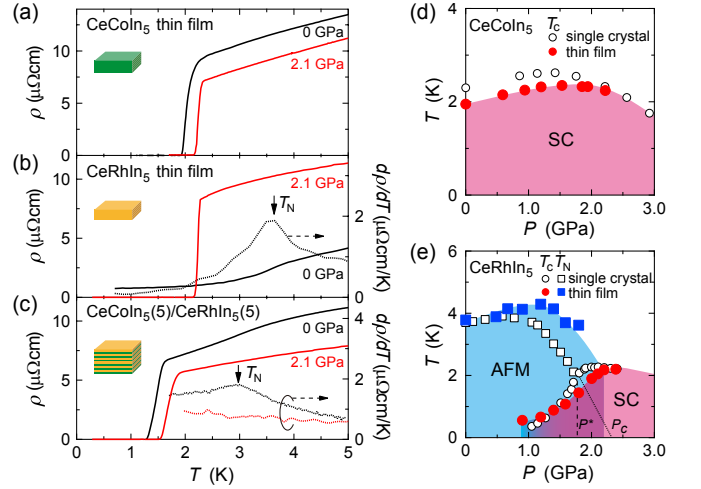


FIG. 9: (a) Temperature dependence of the resistivity of CeCoIn_5 thin film at ambient pressure and at $P = 2.1$ GPa. (b), (c) Temperature dependence of the resistivity (solid lines, left axes) and its temperature derivative $d\rho(T)/dT$ (dotted lines, right axes) for CeRhIn_5 thin film and $\text{CeCoIn}_5(5)/\text{CeRhIn}_5(5)$ superlattice at ambient pressure and at $P = 2.1$ GPa, respectively. The peak of $d\rho(T)/dT$ corresponds to AFM transition. (d), (e) $P - T$ phase diagrams of thin films and single crystals of (d) CeCoIn_5 and (e) CeRhIn_5 .

Figures 9(a), (b) and (c) depict the temperature dependence of the resistivity and its temperature derivative, $d\rho/dT$, for CeCoIn_5 and CeRhIn_5 thin films and $\text{CeCoIn}_5(5)/\text{CeRhIn}_5(5)$ superlattice at ambient and under pressure ($P = 2.1$ GPa), respectively. The peak of $d\rho/dT$ corresponds to the AFM transition. The pressure

dependence of T_c and T_N for CeCoIn₅ and CeRhIn₅ thin films, along with those for single crystals, are shown in Figs 9(d) and 9(e). The $P - T$ phase diagrams of both films are essentially similar to those of single crystals. However, T_c ($= 2.0$ K) in the CeCoIn₅ thin film is slightly reduced from the bulk value, whereas T_N ($= 3.7$ K) of CeRhIn₅ thin film is almost the same as that in a single crystal. With applying pressure, T_c of the CeCoIn₅ thin film increases and shows a broad peak near $P \sim 1.7$ GPa. Similar to CeRhIn₅ single crystals [13, 102], superconductivity in the thin films develops at $P \gtrsim 1$ GPa, where it coexists with magnetic order. In analogy to CeRhIn₅ single crystals, there appears to be a purely superconducting state at $P \gtrsim 2.1$ GPa, which is a slightly higher pressure than that required to remove evidence for AFM order in single crystals.

Figure 10(a) shows the P -dependence of T_c and T_N determined by the peak in $d\rho(T)/dT$ for CeCoIn₅(5)/CeRhIn₅(5) superlattice. At $P \sim 2$ GPa, T_c is at a maximum, forming a dome-shaped P -dependence. With pressure, T_N gradually decreases at low P and decreases sharply when it exceeds $P \gtrsim 1$ GPa. At $P \gtrsim 1.6$ GPa, evidence of magnetic order is hidden beneath the superconducting dome. Although there is large ambiguity in determining a critical pressure P_c , a simple extrapolation of T_N gives $P_c \sim 2$ GPa, where T_c has a maximum. Furthermore, this critical value is very close to the P_c of CeRhIn₅ single crystal.

The T_c and T_N of the hybrid superlattice are lower than those of the CeCoIn₅ and CeRhIn₅ thin films, suggesting that the reduction in dimensions affected the electronic structure. However, these values are higher than the corresponding CeCoIn₅/YbCoIn₅ and CeRhIn₅/YbRhIn₅, indicating the importance of interaction between CeCoIn₅ and CeRhIn₅ BLs.

B. Superconductivity and antiferromagnetism in specially separated layers

We show that 2D superconductivity is realized in the CeCoIn₅ BLs in the whole pressure regime in CeCoIn₅(5)/CeRhIn₅(5) superlattice. Figure 10(b) depicts the T -dependence of the upper critical field determined by the midpoint of the resistive transition in a magnetic field H applied parallel ($H_{c2\parallel}$) and perpendicular ($H_{c2\perp}$) to the ab plane. Figure 10(c) shows the T -dependence of the anisotropy of upper critical fields, $H_{c2\parallel}/H_{c2\perp}$. Unlike the almost T -independent anisotropy seen in single crystals and thin films of CeCoIn₅, anisotropy in the superlattice shows a divergent increase toward T_c . This diverging anisotropy is characteristic of 2D superconductivity, in which $H_{c2\parallel}$ increases as $\sqrt{T_c - T}$ due to the Pauli paramagnetic limiting, but $H_{c2\perp}$ increases as $T_c - T$ due to orbital limiting near T_c . Considering this result and the fact that the 5-UCT of the CeCoIn₅ BL is comparable to the superconducting coherence length in the c -axis direction $\xi_{\perp} \sim 3$ –4 nm, the

5-UCT of the CeCoIn₅ BL effectively act as a 2D superconductor [44]. The 2D superconductivity is also confirmed from the angle variation of $H_{c2}(\theta)$. Figure 10(d) and its inset show $H_{c2}(\theta)$ below and above P^* . For both pressures, at temperature well below T_c , $H_{c2}(\theta)$ in the regime $|\theta| \lesssim 30^\circ$ is enhanced with decreasing $|\theta|$ and exhibits a sharp cusp at $\theta = 0$. This cusp behavior is typical of Josephson-coupled layered superconductors [82].

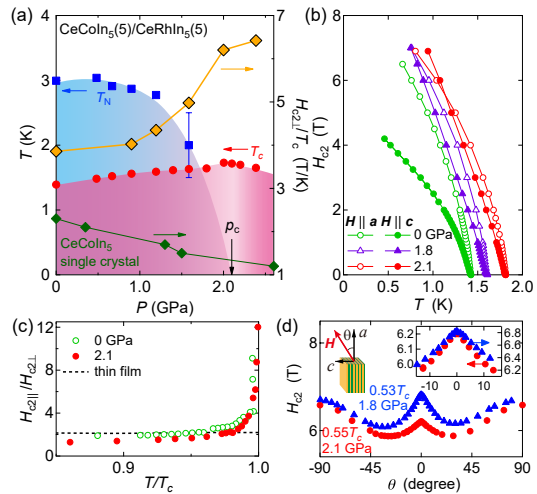


FIG. 10: (a) $P - T$ phase diagram of CeCoIn₅(5)/CeRhIn₅(5) superlattice. Out-of-plane upper critical field $H_{c2\perp}$ normalized by T_c , $H_{c2\perp}/T_c$, measures the coupling strength of the superconductivity. (b) Temperature dependence of in-plane and out-of-plane upper critical fields at ambient pressure and at $P = 1.8$ and 2.1 GPa. (c) Anisotropy of upper critical field, $H_{c2\parallel}/H_{c2\perp}$, near T_c of superlattices at ambient pressure and at 2.1 GPa, along with the data of CeCoIn₅ thin film. (d) Angular dependence of upper critical field of superlattice at $P = 1.8$ and 2.1 GPa. (Inset) An expanded view of low angle region.

It should be noted that in contrast to single crystals and thin films of CeRhIn₅, the CeRhIn₅ layers in CeCoIn₅/CeRhIn₅ hybrid superlattices do not become fully superconducting even under pressure where AFM order is suppressed. As a result, 2D superconductivity occurs in a wide pressure regime. In fact, as shown in Fig. 10(d), at $P = 1.8$ GPa where CeRhIn₅ thin film does not show bulk superconductivity, the hybrid superlattice shows an angular dependence with a cusp structure near $\theta = 0$. Essentially similar cusp-like behavior is observed at $P = 2.1$ GPa above P_c , suggesting that 2D superconductivity derived from the CeCoIn₅ BLs is realized below and above P_c .

When the number of BL thickness is reduced, superconductivity survives in CeCoIn₅, but is suppressed in CeRhIn₅. This difference may be related to the ordering vector $\mathbf{q} = (0.5, 0.5, 0.297)$ [34] of the incommensurate magnetic structure of CeRhIn₅. In CeCoIn₅, on the other hand, the AFM fluctuations are dominated by $\mathbf{q} = (0.45, 0.45, 0.5)$ [59]. This commensurability along the c -axis would match well with the superlattice struc-

ture, and as a result, the superconductivity is robust against the decrease in the BL thickness [47, 103]. Recent site-selective NMR measurements on CeCoIn₅/CeRhIn₅ superlattice have shown that AFM order is not induced in the CeCoIn₅ BLs [104]. The pressure suppresses magnetic order in CeRhIn₅ and CeCoIn₅ approaches the Fermi liquid state, so it is unlikely that AFM order is induced in the CeCoIn₅ BLs in the superlattice under pressure. We comment on the reversal of H_{c2} of the CeCoIn₅(5)/CeRhIn₅(5) superlattice at low temperature under pressure (Fig. 10(b)). Such a reversed anisotropy of H_{c2} can be seen in CeRhIn₅ single crystal in a high pressure region where AFM order is completely suppressed. However, similar reversed anisotropy ($H_{c2\perp} > H_{c2\parallel}$) is preserved at $P = 1.8$ GPa, where $H_{c2\parallel}$ exceeds $H_{c2\perp}$ in CeRhIn₅ single crystal and thin film. This result suggests that the reversal of H_{c2} occurs in 5-UCT CeCoIn₅ BLs. From the above results, we conclude that 2D superconductivity of CeCoIn₅ coupled by the Josephson effect within a BL is realized in the whole pressure regime.

Figure 7 displays $H_{c2\perp}(T)/H_{c2\perp}(0)$ of CeCoIn₅(n)/CeRhIn₅(n) and CeCoIn₅(n)/YbCoIn₅(5) superlattices plotted as a function of T/T_c . Here $H_{c2\perp}^{\text{orb}}(0)$ is calculated by the initial slope of $H_{c2\perp}(T)$ at T_c by using Werthamer-Helfand-Hohenberg (WHH) formula, $H_{c2\perp}^{\text{orb}}(0) = -0.69T_c(dH_{c2\perp}/dT)_{T_c}$. For comparison, we also include two extreme cases: $H_{c2\perp}/H_{c2\perp}^{\text{orb}}(0)$ for bulk CeCoIn₅ [105], in which H_{c2} is dominated by Pauli paramagnetism, and the WHH curve with no Pauli effect. In CeCoIn₅(n)/YbCoIn₅(5), $H_{c2\perp}/H_{c2\perp}^{\text{orb}}(0)$ increases with decreasing n . This is because the local inversion symmetry breaking suppresses the Pauli pair-breaking effect at the interfaces between BLs. As n decreases, the contribution of the interface increases and the relative importance of orbital pair-breaking effect compared with Pauli pair-breaking effect increases. On the other hand, $H_{c2\perp}/H_{c2\perp}^{\text{orb}}$ is almost independent on n in CeCoIn₅(n)/CeRhIn₅(n), suggesting that the local inversion symmetry breaking is not important in the superlattices in which both substances constituting the superlattice are Ce-based compounds.

C. Enhancement of superconducting pairing strength

The superconducting properties of the hybrid superlattice change dramatically when pressure is applied. Figure 11(a) depicts the T -dependence of $H_{c2\perp}/H_{c2\perp}^{\text{orb}}(0)$ of CeCoIn₅(5)/CeRhIn₅(5) for several pressures. Remarkably, near the critical pressure of $P_c \sim 2$ GPa where AFM order vanishes, $H_{c2\perp}/H_{c2\perp}^{\text{orb}}$ almost coincides with WHH curve, indicating that $H_{c2\perp}$ is determined only by the orbital pair-breaking effect.

The fact that $H_{c2\perp}$ reaches the orbital limit has important implications for the superconducting properties of the hybrid superlattice. In CeCoIn₅/YbCoIn₅, where YbCoIn₅ is a conventional metal, Pauli pair-breaking ef-

fect is weakened in the superlattice compared with the bulk due to local inversion symmetry breaking at the interfaces, where the Fermi surface splits with spin momentum locking due to anisotropic Rashba spin-orbit interaction. This leads to anisotropic suppression of the Zeeman effect which may be partly responsible for the observed reversed anisotropy $H_{c2\parallel}/H_{c2\perp} < 1$ at low temperatures (Fig. 10(d)). However, this effect is less important in CeCoIn₅(n)/CeRhIn₅(n) superlattices compared with CeCoIn₅/YbCoIn₅, which is evidenced by the fact that $H_{c2\perp}/H_{c2\perp}^{\text{orb}}(0)$ does not strongly depend on n (Fig. 7). Furthermore, such an effect is not expected to show significant pressure dependence. Therefore, there must be a different mechanism that significantly enhances $H_{c2\perp}^{\text{Pauli}}$ given by Eq. (1).

An enhancement of $H_{c2\perp}^{\text{Pauli}}$ is not due to a dramatic suppression of g . As g is enhanced by pressure in both CeCoIn₅ and CeRhIn₅ [102], g is expected to be enhanced with pressure in the superlattice. Therefore, a significant increase in the superconducting gap is thought to be the origin of the increase in $H_{c2\perp}^{\text{Pauli}}$. This is also supported by the sharp increase in $H_{c2\perp}/T_c$ upon approaching P_c shown in Fig. 11(a). Because $H_{c2\perp} \approx H_{c2\perp}^{\text{Pauli}} \ll H_{c2\perp}^{\text{orb}}(0)$ in the low P regime and $H_{c2\perp} \approx H_{c2\perp}^{\text{orb}}(0) \ll H_{c2\perp}^{\text{Pauli}}$ near $P \sim p_c$, the enhancement of $H_{c2\perp}/k_B T_c$ directly indicates an enhancement of $H_{c2\perp}^{\text{Pauli}}/T_c$ and hence $\Delta/k_B T_c$. This behavior is significantly different from CeCoIn₅ single crystal, in which $H_{c2\perp}/T_c$ monotonically decreases with pressure, approaching the Fermi liquid state. The enhancement of $\Delta/k_B T_c$ is caused as a consequence of the enhancement of pairing interaction. In the spin fluctuation mediated mechanism, the pairing interaction is brought about by high-energy spin fluctuations well above Δ , while low-energy fluctuations cause the pair-breaking. High-energy fluctuations have the effect of increasing T_c , while low-energy fluctuations decrease T_c , so that the enhancement of pairing interaction can give rise to increase in $\Delta/k_B T_c$ without accompanying a large enhancement of T_c . Therefore, these results demonstrate that the critical magnetic fluctuations developed in CeRhIn₅ BLs near its critical pressure are injected into CeCoIn₅ BLs through the interface and enhance the pairing interaction of the CeCoIn₅ BLs.

It has been established that normal and superconducting properties are greatly affected by quantum fluctuations in many classes of unconventional superconductors. The common behavior is that the effective mass of quasiparticle diverges as the system approaches a QCP, as reported in cuprates, pnictides and heavy-fermion systems [16, 38, 106]. Such an increase in effective mass gives rise to a corresponding enhancement H_{c2}^{orb} , which is proportional to $(m^* \Delta)^2$. The CeCoIn₅/CeRhIn₅ superlattices show different behavior. In contrast to the CeRhIn₅ single crystal, which shows a sharp peak at the critical pressure, the $H_{c2\perp}^{\text{orb}}$ of the CeCoIn₅(n)/CeRhIn₅(n) superlattices with $n = 4$ and 5 does not show much P -dependent behavior, and there is no anomaly in P_c . Compared to a monotonic decrease of effective mass in CeCoIn₅ single

crystal, the result of the hybrid superlattice is consistent with an enhancement of Δ , indicating that there is no mass enhancement in CeCoIn₅ BLs. Such behavior is in contrast to what is expected for usual quantum criticality, and is a subject for future research.

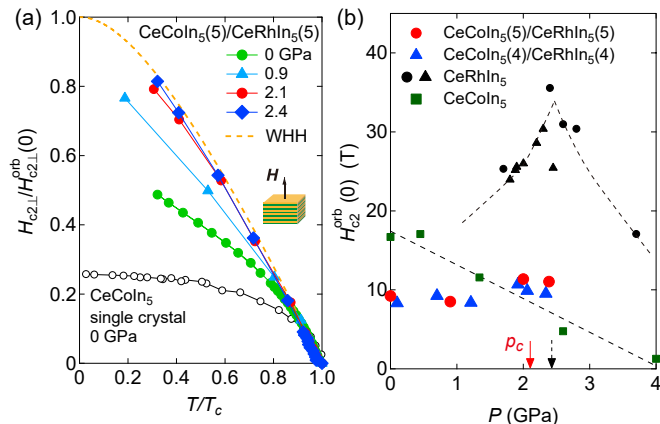


FIG. 11: (a) Out-of-plane upper critical field $H_{c2\perp}$ normalized by the orbital-limited upper critical field at $T = 0$ K, $H_{c2\perp}/H_{c2\perp}^{\text{orb}}(0)$, for CeCoIn₅(5)/CeRhIn₅(5) superlattice is plotted as a function of the normalized temperature T/T_c . Two extreme cases, i.e., the result of the bulk CeCoIn₅ dominated by Pauli paramagnetic effect and the WHH curve with no Pauli effect, are also shown. (b) Pressure dependence of $H_{c2}^{\text{orb}}(0)$ of CeCoIn₅(n)/CeRhIn₅(n) superlattices with $n = 4$ and 5 for $\mathbf{H}\parallel c$. For comparison, $H_{c2}^{\text{orb}}(0)$ of CeRhIn₅ single crystals for $\mathbf{H}\parallel a$ and that of CeCoIn₅ single crystal for $\mathbf{H}\parallel c$ are shown. Solid and dashed arrows represent P_c for CeCoIn₅(n)/CeRhIn₅(n) superlattices and CeRhIn₅ single crystal, respectively.

VI. COUPLING BETWEEN SUPERCONDUCTIVITY AND ANTIFERROMAGNETISM

To further examine how d -wave superconductors and antiferromagnets interact through the interface, we designed another hybrid superlattice using a different AFM metal CeIn₃ [49]. The cubic CeIn₃ forms 3D AFM order with the ordered magnetic moment of $0.48 \mu_B$ occurs with a commensurate wave vector $\mathbf{q} = (0.5, 0.5, 0.5)$ at $T_N = 10$ K, where μ_B is the Bohr magneton [72]. This is contrast to CeRhIn₅, which forms an incommensurate helical AFM order with $\mathbf{q} = (0.5, 0.5, 0.239)$ at $T_N = 2.3$ K. On the other hand, both are Ce-based heavy-fermion AFM metal with AFM QCP under pressure [10, 74]. Therefore, it becomes possible to investigate the effect of different types of antiferromagnetism on d -wave superconductivity by measuring the H_{c2} for CeCoIn₅/CeIn₃ superlattice under pressure, as have done for CeCoIn₅/CeRhIn₅.

A. Robust magnetism against thickness reduction

Figure 12(a) depicts the temperature dependence of the resistivity ρ of CeCoIn₅(7)/CeIn(n) superlattices with $n = 3, 4, 6$ and 13. We also show ρ of CeCoIn₅ and CeIn₃ thin films grown by MBE. The mean free path of these superlattices is difficult to estimate because of the parallel conduction of CeCoIn₅ and CeIn₃ BLs. However, the mean free path in each BL is expected to be shorter than the atomically flat regions extending over distances of $\sim 0.1 \mu\text{m}$, because of the following reasons. In CeCoIn₅ and CeIn₃ single crystals, the mean free path determined by the de Haas-van Alphen oscillations is $\sim 0.2 \mu\text{m}$ [107, 108]. The residual resistivity ratio of CeCoIn₅ and CeIn₃ thin films with 100 nm thickness is 4–5 times smaller than that of the single crystals. Therefore, the mean free path of CeCoIn₅ and CeIn₃ BLs in the superlattices is expected to be much shorter than $0.1 \mu\text{m}$, suggesting that the transport properties are not seriously influenced by the surface roughness. The resistivity of CeCoIn₅(7)/CeIn(n) superlattices follows the typical heavy-fermion behavior. With decreasing temperature, $\rho(T)$ increases below ~ 150 K due to the Kondo scattering but then begins to decrease due to strong c - f hybridization between f -electrons and conduction (c) band electrons, leading to the narrow f -electron band at the Fermi level. The Kondo coherence temperature T_{coh} , at which the formation of heavy-fermion occurs, is estimated from the maximum in $\rho(T)$. As shown in Fig. 12(a), T_{coh} of CeCoIn₅(7)/CeIn(n) superlattices is nearly independent of n and is closer to T_{coh} of CeCoIn₅ thin film than T_{coh} of CeIn₃ thin film, suggesting that T_{coh} is mainly determined by CeCoIn₅ BLs. Figure 12(b)-(f) depict $\rho(T)$ at low temperatures. All superlattices show the superconducting transition at $T \approx 1.5$ K. For the $n = 3$ - and 4-superlattices, $\rho(T)$ decreases with increasing slope, $d\rho(T)/dT$, as the temperature is lowered below 12 K down to T_c .

The lattice parameters along the a -axis of CeCoIn₅, CeRhIn₅, and CeIn₃ is 4.613, 4.653, and 4.690 Å, respectively. Therefore, a large tensile strain along the a -axis is expected in CeCoIn₅ BLs of CeCoIn₅/CeIn₃ compared to CeCoIn₅/CeRhIn₅. It has been shown that the uniaxial pressure dependence of T_c along the a -axis for CeCoIn₅ is $dT_c/dP_a = 290$ mK/GPa ([109]), indicating that T_c decreases by tensile strain. However, T_c of CeCoIn₅/CeIn₃ ($T_c \sim 1.5$ K) is larger than that of CeCoIn₅/CeRhIn₅ ($T_c \sim 1.4$ K). We note that the lattice parameter along the c -axis for CeCoIn₅ BLs in CeCoIn₅/CeIn₃, which is estimated from x-ray diffraction, well coincides with that in CeCoIn₅/CeRhIn₅. These results suggest that the strain effect at the interfaces is not important for determining T_c . Figure 12(g)-(k) display the temperature derivative of the resistivity $d\rho(T)/dT$. As shown by the arrows in Fig. 12(g), $d\rho(T)/dT$ of CeIn₃ thin film exhibits a distinct kink at $T_N = 10$ K [72]. Similar kink structures are observed in all superlattices at the temperatures indicated by arrows, showing the AFM tran-

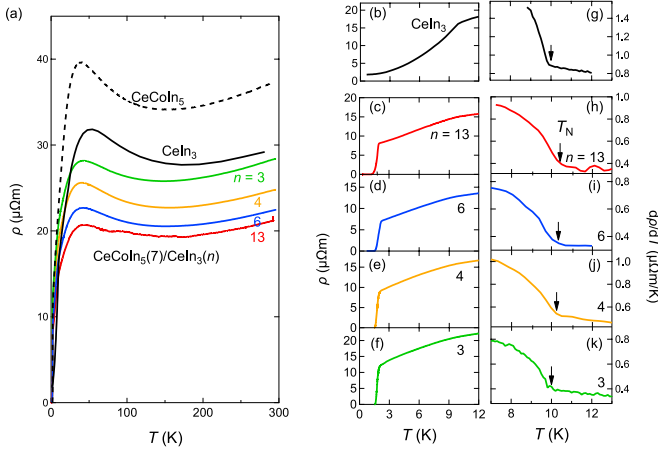


FIG. 12: (a) Temperature dependence of the resistivity $\rho(T)$ in $\text{CeCoIn}_5(7)/\text{CeIn}_3(n)$ superlattices for $n = 3, 4, 6,$ and 13 , along with $\rho(T)$ for CeIn_3 (black solid line) and CeCoIn_5 (black dashed line) thin films. Inset illustrates the schematics of $\text{CeCoIn}_5(7)/\text{CeIn}_3(n)$ superlattice. (b)-(f) $\rho(T)$ at low temperatures. (g)-(k) Temperature derivative of the resistivity, $d\rho(T)/dT$, as a function of temperature. The arrows indicate the Néel temperature T_N .

sition. Figure 13 shows the thickness dependence of T_N

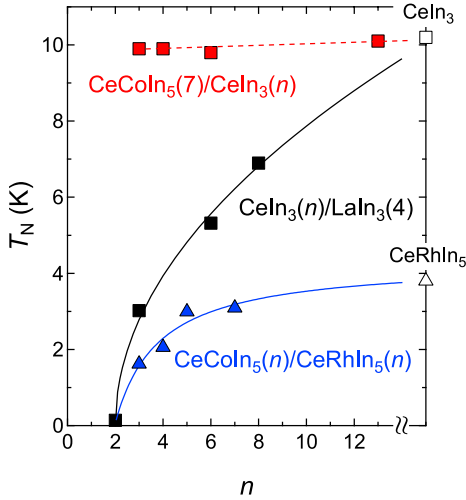


FIG. 13: The Néel temperature T_N for $\text{CeCoIn}_5(7)/\text{CeIn}_3(n)$ as a function of n . For comparison, T_N for $\text{CeIn}_3(n)/\text{LaIn}_3(4)$ and $\text{CeCoIn}_5(n)/\text{CeRhIn}_5(n)$ are shown. Open square and triangle are T_N of bulk CeIn_3 and CeRhIn_5 single crystals, respectively.

of the $\text{CeCoIn}_5(7)/\text{CeIn}_3(n)$ superlattices. For comparison, the data sets of $\text{CeIn}_3(4)/\text{LaIn}_3(n)$, where LaIn_3 is a nonmagnetic conventional metal with no f -electrons [50], and $\text{CeCoIn}_5(n)/\text{CeRhIn}_5(n)$ are also included in Fig. 13. Remarkably, the observed thickness dependence of T_N in $\text{CeCoIn}_5/\text{CeIn}_3$ is in striking contrast to that in $\text{CeIn}_3/\text{LaIn}_3$; While T_N is strongly suppressed with decreasing n and vanishes at $n = 2$ in $\text{CeIn}_3/\text{LaIn}_3$,

T_N is nearly independent of n in $\text{CeCoIn}_5(7)/\text{CeIn}_3(n)$. This suggests that CeIn_3 BLs are coupled weakly by the RKKY interactions through the adjacent LaIn_3 BL, but they can strongly couple through the adjacent CeCoIn_5 BL. This is even more surprising, as the distance between different CeIn_3 BLs is larger in the $\text{CeCoIn}_5(7)/\text{CeIn}_3(n)$ superlattices than in the $\text{CeIn}_3(n)/\text{LaIn}_3(4)$ superlattices. We thus conclude that small but finite magnetic moments are induced in CeCoIn_5 BLs in $\text{CeCoIn}_5/\text{CeIn}_3$, which mediate the RKKY-interaction. On the other hand, because of the absence of strongly interacting f -electrons in LaIn_3 , which can form magnetic moments, the RKKY interaction in $\text{CeIn}_3/\text{LaIn}_3$ can be expected to be much weaker. To clarify this, a microscopic probe of magnetism, such as NMR measurements, is required. We note that as shown in Fig. 13, the reduction of T_N is also observed in $\text{CeCoIn}_5(n)/\text{CeRhIn}_5(n)$ superlattices [48], suggesting that the RKKY interaction between CeRhIn_5 BLs through adjacent CeCoIn_5 BL is negligibly small. This is supported by the recent site-selective NMR measurements which report no discernible magnetic moments induced in the CeCoIn_5 BLs while magnetic fluctuations are injected from CeRhIn_5 BLs into one or two layers of CeCoIn_5 BLs in $\text{CeCoIn}_5/\text{CeRhIn}_5$ [104].

B. Tuning AFM fluctuations via pressure

The pressure dependence of the superconducting and magnetic properties provide crucial information on the mutual interaction between superconductivity and magnetism through the interface. Figure 14(a) depicts the pressure dependence of T_N and T_c for $\text{CeCoIn}_5(7)/\text{CeIn}_3(n)$ superlattices for $n = 6$ and 13 . With applying pressure, T_N decreases rapidly. For comparison, T_N of a single crystal CeIn_3 is also shown by the solid line [10]. The pressure dependence of T_N of both superlattices is very similar to that of the bulk CeIn_3 single crystal. In bulk CeIn_3 crystal, the AFM QCP is located at $P_c \approx 2.6$ GPa. It is natural to expect, therefore, that the AFM QCP of the superlattices is close to 2.6 GPa. Thus, at 2.4 GPa, the superlattices are in the vicinity of the AFM QCP. This is supported by the temperature dependence of the resistivity under pressure. The resistivity can be fitted as

$$\rho(T) = \rho_0 + AT^\varepsilon. \quad (6)$$

Figure 14(b) shows the pressure dependence of ε obtained from $d \ln \Delta\rho / d \ln T$, where $\Delta\rho = \rho(T) - \rho_0$. The magnitude of ε decreases with pressure. In bulk CeIn_3 single crystal, ε decreases with pressure and exhibits a minimum at the AFM QCP [10, 74]. On the other hand, applying pressure to CeCoIn_5 leads to an increase of ε , which is attributed to the suppression of the non-Fermi liquid behavior, $\rho(T) \propto T$, and the development of a Fermi liquid state with its characteristic $\rho(T) \propto T^2$ dependence [32, 33]. Therefore, the reduction of ε with

pressure arises from the CeIn₃ BLs, indicating that the CeIn₃ BLs approach the AFM QCP.

As shown in Fig14(a), T_c increases, peaks at ~ 1.8 GPa, and then decreases when applying pressure. This pressure dependence bears a resemblance to that of CeCoIn₅ bulk single crystals [32]. An analysis of the upper critical field provides important information about the superconductivity of CeCoIn₅ BLs. Figure 15 depicts the temperature dependence of the upper critical field determined by the midpoint of the resistive transition in a magnetic field \mathbf{H} applied parallel ($H_{c2\parallel}$) and perpendicular ($H_{c2\perp}$) to the layers. The inset of Fig 15 shows the anisotropy of the upper critical fields $H_{c2\parallel}/H_{c2\perp}$ at ambient pressure. The 2D feature is revealed by the diverging anisotropy of $H_{c2\parallel}/H_{c2\perp}$ of the superlattice on approaching T_c , in sharp contrast to the CeCoIn₅ thin film. Thus, each CeCoIn₅ BL in CeCoIn₅/CeIn₃ superlattice effectively behaves as a 2D superconductor.

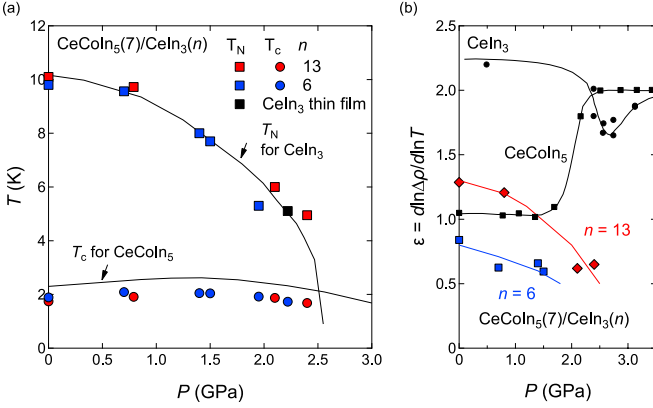


FIG. 14: (a) Pressure dependence of T_N and T_c of CeCoIn₅(7)/CeIn₃(n) superlattices for $n = 13$ and 6. For comparison, T_N of CeIn₃ and T_c of CeCoIn₅ single crystals are shown by solid lines. (b) Pressure dependence of the exponent ϵ in $\rho(T) = \rho_0 + AT^\epsilon$, obtained from $d \ln \Delta \rho / d \ln T$ ($\Delta \rho = \rho(T) - \rho_0$), for the CeCoIn₅(7)/CeIn₃(n) superlattices for $n = 13$ and 6. For comparison, ϵ for bulk CeIn₃ and CeCoIn₅ single crystals is shown.

C. Effect of magnetic fluctuations on superconductivity

It has been revealed that the T dependence of $H_{c2\perp}$ provides crucial information on the effect of interfaces on the superconductivity of CeCoIn₅ BLs. In particular, the modification of the Pauli paramagnetic effect in the superlattice, which dominates the pair breaking in bulk CeCoIn₅ single crystals, provide valuable clues [45, 46, 48, 91]. Figure 16(a) and (b) depict the T dependence of the $H_{c2\perp}$ of CeCoIn₅(7)/CeIn₃(13) superlattice at ambient pressure Fig. 16(a) and under pressure Fig. 16(b), normalized by the orbital-limited upper critical field at zero temperature, $H_{c2\perp}^{\text{orb}}(0)$, which is obtained from the WHH formula, $H_{c2\perp}^{\text{orb}}(0) = -0.69T_c(dH_{c2\perp}/dT)_{T_c}$ [84].

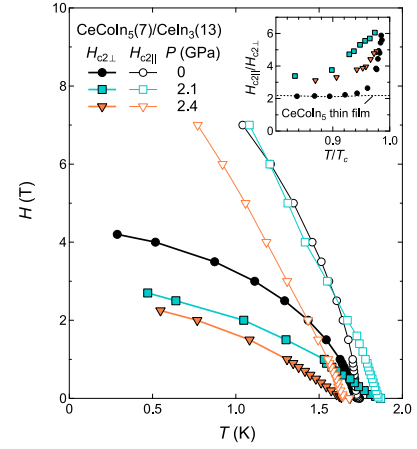


FIG. 15: Temperature dependence of upper critical fields in magnetic fields parallel ($H_{c2\parallel}$, open symbols) and perpendicular ($H_{c2\perp}$, closed symbols) to the ab -plane for CeCoIn₅(7)/CeIn₃(13) superlattice at ambient pressure and at 2.1 and 2.4 GPa. The inset shows anisotropy of the upper critical field, $H_{c2\parallel}/H_{c2\perp}$. The data of CeCoIn₅ thin film at ambient pressure is shown by dotted line.

In figure 16(a) and 16(b), two extreme cases are also included; the WHH curve with no Pauli pair-breaking and $H_{c2}/H_{c2\perp}^{\text{orb}}(0)$ for bulk CeCoIn₅ single crystal [105]. For comparison, $H_{c2\perp}^{\text{orb}}(0)$ for CeCoIn₅/YbCoIn₅ and CeCoIn₅/CeRhIn₅ are also shown [44, 48].

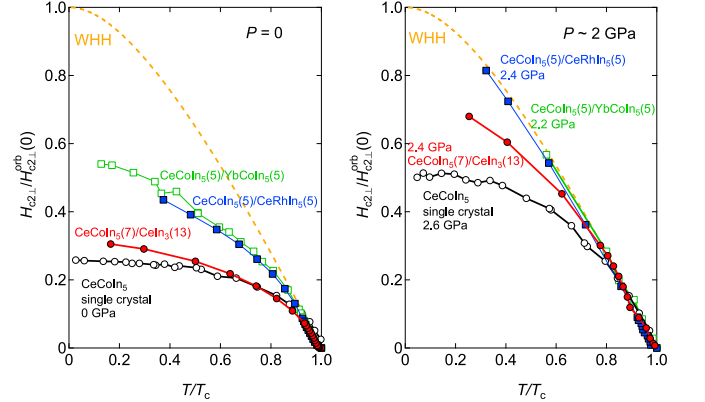


FIG. 16: (a) Upper critical field in perpendicular field normalized by the orbital limiting upper critical field, $H_{c2\perp}/H_{c2\perp}^{\text{orb}}(0)$, plotted as a function of T/T_c (a) at ambient pressure and (b) under pressure about 2 GPa for CeCoIn₅(7)/CeIn₃(13) superlattices. For comparison, $H_{c2\perp}/H_{c2\perp}^{\text{orb}}(0)$ for bulk CeCoIn₅ single crystal, CeCoIn₅(5)/YbCoIn₅(5) and CeCoIn₅(5)/CeRhIn₅(5) are shown. Orange dotted lines represent the WHH curve, which is upper critical field for purely orbital limiting.

At ambient pressure, $H_{c2\perp}/H_{c2\perp}^{\text{orb}}(0)$ is significantly increased from bulk CeCoIn₅ single crystal in both CeCoIn₅/YbCoIn₅ and CeCoIn₅/CeRhIn₅, indicating the suppression of the Pauli paramagnetic pair-breaking effect. However, we point out that the mechanisms of this

suppression in these two systems are essentially different. In CeCoIn₅/YbCoIn₅, as discussed in section IV-B, the enhancement of $H_{c2\perp}/H_{c2\perp}^{\text{orb}}(0)$ is caused by the local ISB at the interface [45, 86]. At $P = 2.2$ GPa, $H_{c2\perp}/H_{c2\perp}^{\text{orb}}(0)$ of CeCoIn₅/YbCoIn₅ nearly coincides with the WHH curve, indicating that $H_{c2\perp}$ is dominated by the orbital pair breaking most likely due to the suppression of the Pauli paramagnetic pair-breaking effect by the Rashba splitting.

As shown in Fig. 7, in stark contrast to CeCoIn₅(n)/YbCoIn₅(n), where $H_{c2\perp}/H_{c2\perp}^{\text{orb}}(0)$ is strongly enhanced with decreasing n , $H_{c2\perp}/H_{c2\perp}^{\text{orb}}(0)$ in CeCoIn₅(n)/CeRhIn₅(n) is independent of n . This indicates that the effect of the local ISB on $H_{c2\perp}$ is much less important in CeCoIn₅/CeRhIn₅ than CeCoIn₅/YbCoIn₅, possibly owing to smaller asymmetric potential gradient at Ce/Ce interface compared with that at Ce/Yb one [48]. It has been proposed that magnetic fluctuations in CeRhIn₅ BLs injected through the interface dramatically enhance the pairing interaction in CeCoIn₅ BLs, leading to the enhancement of Δ . As a result, $H_{c2\perp}^{\text{Pauli}}$ is enhanced. This raises the relative importance of the orbital pair-breaking effect, giving rise to the enhancement of $H_{c2\perp}/H_{c2\perp}^{\text{orb}}(0)$ [48]. At $P = 2.1$ GPa, which is close to the AFM QCP of CeRhIn₅ BLs, $H_{c2\perp}/H_{c2\perp}^{\text{orb}}(0)$ nearly coincides with the WHH curve. This has been attributed to the enhanced Pauli limiting field that well exceeds the orbital limiting field ($H_{c2\perp}^{\text{Pauli}} \gg H_{c2\perp}^{\text{orb}}$).

In contrast to CeCoIn₅/YbCoIn₅ and CeCoIn₅/CeRhIn₅, $H_{c2\perp}/H_{c2\perp}^{\text{orb}}(0)$ only show a slight increase from CeCoIn₅(7)/CeIn₃(13) superlattice at ambient pressure from that of bulk CeCoIn₅ single crystal. This indicates that $H_{c2\perp}$ is dominated by Pauli paramagnetic effect, i.e. $H_{c2\perp} \approx H_{c2\perp}^{\text{Pauli}} \ll H_{c2\perp}^{\text{orb}}$. This implies that the effect of local inversion symmetry breaking on the superconductivity in CeCoIn₅/CeIn₃ is weak compared with CeCoIn₅/YbCoIn₅. The local inversion symmetry is broken for the CeCoIn₅/YbCoIn₅ on the CoIn-layer while it is broken on the Ce layer for CeCoIn₅/CeIn₃ and CeCoIn₅/CeRhIn₅. Therefore, the present results suggest that the inversion symmetry breaking on the CoIn-layer induces a larger local electric field gradient. Moreover, superconducting electrons in CeCoIn₅ BLs are not strongly influenced by the AFM order in CeIn₃ BLs compared with CeCoIn₅/CeRhIn₅.

When superconductivity is dominated by the Pauli-limiting effect ($H_{c2\perp} \approx H_{c2\perp}^{\text{Pauli}}$), $2\Delta/k_{\text{B}}T_c$ is obtained from Eq. (1) as

$$\frac{2\Delta}{k_{\text{B}}T_c} \approx \sqrt{2} \frac{g\mu_{\text{B}}H_{c2\perp}}{k_{\text{B}}T_c}. \quad (7)$$

where μ_{B} is Bohr magneton and g is the g -factor of electron. In Fig. 17, $g = 2$ is assumed. Figure 17 depicts the pressure dependence of $q = \sqrt{2}g\mu_{\text{B}}H_{c2\perp}/k_{\text{B}}T_c$ for CeCoIn₅/CeRhIn₅ and CeCoIn₅/CeIn₃, along with q for bulk CeCoIn₅ single crystal. Here $g = 2$ is assumed. Although this simple assumption should be scrutinized, the

fact that $q = 4.2$ of the bulk CeCoIn₅ is larger than the BCS value of $q = 3.54$ is consistent with the strong coupling superconductivity, which is supported by the specific heat measurements that report $2\Delta/k_{\text{B}}T_c \approx 6$ [52]. The increase of q with pressure in CeCoIn₅/CeRhIn₅ implies the increase of $2\Delta/k_{\text{B}}T_c$. This increase has been attributed to an enhancement of the force binding superconducting electron pairs. In this case, an increase of $2\Delta/k_{\text{B}}T_c$ occurs without accompanying a large enhancement of T_c , which is consistent with the results of CeCoIn₅/CeRhIn₅ [48]. Thus, the critical AFM fluctuations that develop in CeRhIn₅ BLs near the QCP are injected into the CeCoIn₅ BLs through the interface and strongly enhance the pairing interaction in CeCoIn₅ BLs.

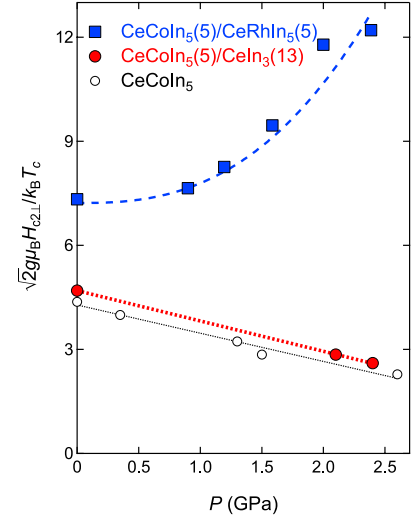


FIG. 17: Pressure dependence of $q = \sqrt{2}g\mu_{\text{B}}H_{c2\perp}/k_{\text{B}}T_c \approx 2\Delta/k_{\text{B}}T_c$ for CeCoIn₅(7)/CeIn₃(13) superlattice. For comparison, q of bulk CeCoIn₅ single crystal and CeCoIn₅(5)/CeRhIn₅(5) are plotted.

In stark contrast to CeCoIn₅/CeRhIn₅ superlattices, q decreases with pressure in bulk CeCoIn₅ single crystal. This implies that the pairing interaction is weakened by applying pressure, which is consistent with the fact that the pressure moves the system away from the QCP of CeCoIn₅. The reduction of $2\Delta/k_{\text{B}}T_c$ with pressure in bulk CeCoIn₅ single crystals is confirmed by the jump of the specific heat at T_c [57]. It should be stressed that the pressure dependence of q in CeCoIn₅(7)/CeIn₃(13) is very similar to that of bulk CeCoIn₅. This strongly indicates that the pairing interactions in CeCoIn₅ BLs are barely influenced by AFM fluctuations injected from the adjacent CeIn₃ BLs through the interface even when CeIn₃ BLs are located near the AFM QCP.

The most salient feature in the CeCoIn₅/CeIn₃ superlattices is that the superconductivity of CeCoIn₅ BLs is little affected by the critical AFM fluctuations in CeIn₃ BLs, despite the fact that AFM fluctuations are injected from the adjacent CeIn₃ BLs into CeCoIn₅ BLs, as evidenced by the AFM order in CeCoIn₅/CeIn₃ demonstrating that different CeIn₃ BLs are magnetically coupled by

the RKKY interaction through adjacent CeCoIn₅ BLs. Even in the vicinity of the AFM QCP of the CeIn₃ BLs, the superconducting state in the CeCoIn₅ BLs is very similar to that of CeCoIn₅ bulk single crystals. This indicates that the AFM fluctuations injected from CeIn₃ BLs do not help to enhance the force binding the superconducting electron pairs in CeCoIn₅ BLs. This is in stark contrast to CeCoIn₅/CeRhIn₅, in which the pairing force in CeCoIn₅ BL is strongly enhanced by the AFM fluctuations in CeRhIn₅ BLs [48], although the CeRhIn₅ BLs are magnetically only weakly coupled through CeCoIn₅ BLs.

We note that the superconducting phase appears under pressure in CeRhIn₅ single crystals and epitaxial thin films. On the other hand, in the CeRhIn₅/YbRhIn₅, zero resistivity is not attained even under pressure [48]. This result indicates that the superconductivity of CeRhIn₅ is suppressed when the thickness of the BLs was reduced. Similarly, in CeCoIn₅/CeRhIn₅ superlattices, 2D superconductivity derived from the CeCoIn₅ BLs is thought to be realized from ambient pressure to under pressure near QCP.

D. Contrasting behaviors between CeCoIn₅/CeIn₃ and CeCoIn₅/CeRhIn₅ superlattices

As discussed in the previous sections, CeCoIn₅/CeIn₃ and CeCoIn₅/CeRhIn₅ superlattices exhibit contrasting superconducting and magnetic properties. We point out that there are two possible important factors that determine whether magnetic fluctuations are injected through the interface; One is the magnetic wave vector and the other is the matching of the Fermi surface between two materials.

For CeCoIn₅, the Fermi surface is 2D-like and AFM fluctuations with wave vector $\mathbf{q}_0 = (0.45, 0.45, 0.5)$ are dominant [59]. The magnetic wave vector in the ordered phase of CeIn₃ is commensurate with $\mathbf{q}_0 = (0.5, 0.5, 0.5)$ [72]. The evolution of the ordered moment below T_N is consistent with mean field theory. While the wave number along the c axis, q_c , of CeIn₃ is the same as that of CeCoIn₅, the 3D Fermi surface of CeIn₃ is very different from the 2D Fermi surface of CeCoIn₅. On the other hand, for CeRhIn₅, \mathbf{q}_0 in the ordered phase is incommensurate $\mathbf{q}_0 = (0.5, 0.5, 0.297)$ at low pressure [34] and changes to $\mathbf{q}_0 = (0.5, 0.5, 0.4)$ above ~ 1.0 GPa [110]. Thus, the q_c of CeRhIn₅ is different from the q_c of CeCoIn₅. The evolution of the ordered moment below T_N deviates from mean field behavior, likely due to 2D fluctuations. However, the 2D Fermi surface of CeRhIn₅ bears a close resemblance to that of CeCoIn₅.

The equality between the c axis component of \mathbf{q}_0 in CeCoIn₅ and CeIn₃ would explain why the magnetic coupling between CeIn₃ BLs through a CeCoIn₅ BL is stronger than that between CeRhIn₅ BLs. Thus, AFM order is formed in CeCoIn₅(7)/CeIn₃(n) even for small n , for which the AFM order has already vanished in

CeCoIn₅(n)/CeRhIn₅(n). In magnetically mediated superconductors, the pairing interaction is expected to be strongly wave number dependent. Considering the good resemblance of the Fermi surface and the same $d_{x^2-y^2}$ superconducting gap symmetry of CeCoIn₅ and CeRhIn₅ [102], it is likely that the pairing interaction in both compounds has 2D character and peaks around the same wave number on the Fermi surface. Furthermore, it has been assumed that 2D magnetic fluctuations are strong in CeRhIn₅. Thus, superconductivity in the CeCoIn₅ BLs of CeCoIn₅(n)/CeRhIn₅(n) is strongly influenced. On the other hand, in CeIn₃ with 3D Fermi surface, 2D AFM fluctuations are expected to be very weak. AFM fluctuations having 3D character in CeIn₃ may not play an important role for the pairing interaction in CeCoIn₅, resulting in little change of the superconductivity in CeCoIn₅/CeIn₃.

VII. CONCLUSION

We reviewed the most recent advances of Kondo superlattices containing atomic layers of strongly correlated heavy fermion superconductor CeCoIn₅ with d -wave symmetry, CeCoIn₅/YbCoIn₅, CeCoIn₅/CeRhIn₅ and CeCoIn₅/CeIn₃ grown by using a state-of-the-art MBE technique. In these Kondo superlattices, superconducting heavy electrons are confined within the 2D CeCoIn₅ block layers and interact with the neighboring nonmagnetic or magnetic layers through the interface.

In CeCoIn₅/YbCoIn₅ superlattices, the superconductivity is strongly influenced by the local ISB at the interface, which seriously reduces the Pauli paramagnetic pair-breaking effect. Our results demonstrate that the tricolor Kondo superlattices provide a new playground for exploring exotic superconducting states in the strongly correlated 2D electron systems with the Rashba effect.

CeCoIn₅/CeRhIn₅ and CeCoIn₅/CeIn₃ superlattices, the superconducting and antiferromagnetic states coexist in spatially separated layers, but their mutual coupling via the interface significantly modifies the superconducting and magnetic properties. In CeCoIn₅/CeRhIn₅ superlattices, the superconductivity in the CeCoIn₅ BLs is profoundly affected by AFM fluctuations in the CeRhIn₅ BLs. Upon suppressing the AFM order by applied pressure, the force binding superconducting electron pairs acquires an extreme strong coupling nature, highlighting that the pairing interaction can be maximized by the critical fluctuations emanating from the magnetic QCP. In CeCoIn₅/CeIn₃ superlattices, each CeIn₃ BL is magnetically coupled by RKKY interaction through the adjacent CeCoIn₅ BLs. In stark contrast to CeCoIn₅/CeRhIn₅ superlattices, the superconductivity in the CeCoIn₅ BLs in CeCoIn₅/CeIn₃ superlattices is barely influenced by the AFM fluctuations in the CeIn₃ BLs, even when the CeIn₃ BLs are tuned in the vicinity of the AFM QCP by pressure. The striking difference between the two Kondo

superlattices provides direct evidence that 2D AFM fluctuations are essentially important for the pairing interactions in CeCoIn₅.

Finally, we describe the future prospect of the Kondo superlattices. Cd- and Hg-doped CeCoIn₅ are known to show anomalous antiferromagnetic order at small doping levels[111–113]. The fabrication of superlattices consisting of alternating layers of Cd- and Hg-doped CeCoIn₅ and pure CeCoIn₅ is expected to provide important information on the interplay between superconductivity and unusual magnetic order. The advantage of these superlattices is that the mismatch of the lattice constant is very small. Recently, strongly correlated electron systems with strong Rashba interaction are attracting much attention[114–116]. Thus fabricating superlattices including the noncentrosymmetric heavy fermion superconductors CePt₃Si[117] and pressure-induced superconductors CeRhSi₃[118], CeIrSi₃[119], and heavy fermion superconductors whose inversion symmetry is broken locally around the Ce site CeRh₂As₂[120] will give important information of the interplay between superconductivity and strong Rashba interaction. We also note that the Dzyaloshinskii–Moriya interaction plays an important role for the Kondo effect and magnetic order at the interface between different materials. Theoretical research in this direction appears to be ongoing[121, 122], but the impact on the *f*-electron superlattice is not clear at the moment.

Besides the Kondo superlattices, the present MBE technique enables us to grow monolayer CeCoIn₅ and CeRhIn₅ on the top of the nonmagnetic YbCoIn₅ thin film. It has been proposed theoretically that monolayer CeCoIn₅ forms a topological superconducting state owing to the strong Rashba interaction[98, 99, 123, 124]. Most of the past research on topological superconductivity has focused on weakly correlated materials. The topological superconductivity in monolayer CeCoIn₅ will give an opportunity to study topological excitations, including Majorana fermions in strongly correlated *d*-wave super-

conductors. Moreover, it is an open question whether monolayer CeRhIn₅ exhibits magnetic order. It is highly challenging to study these issues by using the scanning tunneling microscopy measurements.

The fabrication of a wide variety of Kondo superlattices paves a new way to study the entangled relationship between unconventional superconductivity and magnetism in strongly correlated electron systems, offering a route to exploring the emergence of novel superconducting systems and the roles of their interface.

Acknowledgments

The authors acknowledge collaborations with Yongkang Luo, P. F. S. Rosa, F. Ronning, J. D. Thompson, K. Ishida, T. Yamanaka, G. Nakamine, S. Miyake, S. Nakamura, T. Ishii, R. Peters, Y. Tokiwa, Y. Kasahara, and T. Shibauchi. We thank H. Kontani and Y. Yanase for valuable discussion. This work was supported by Grants-in-Aid for Scientific Research (KAKENHI) (No.25220710, No.18J10553, and No.18H05227) and Innovative Areas "Topological Material Science" (No.JP15H05852) and "3D Active-Site Science" (No.26105004) from the Japan Society for the Promotion of Science (JPSJ) and JST CREST (No. JP-MJCR18T2).

Data Availability

The data that support the findings of this study are available from American Physical Society. Restrictions apply to the availability of these data, which were used under license for this study. Data are available from the authors upon reasonable request and with the permission of American Physical Society.

-
- [1] D. J. Scalapino, Rev. Mod. Phys. **84**, 1383 (2012).
 [2] B. Keimer, S. A. Kivelson, M. R. Norman, S. Uchida, and J. Zaanen, Nature **518**, 179 (2015).
 [3] P. J. Hirschfeld, M. M. Korshunov, and I. I. Mazin, Rep. Prog. Phys. **74**, 124508 (2011).
 [4] G. R. Stewart, Advances in Physics **66**, 75 (2017).
 [5] T. Shibauchi, T. Hanaguri, and Y. Matsuda, J. Phys. Soc. Jpn. **89**, 102002 (2020).
 [6] P. Thalmeier and G. Zwicknagl, *Unconventional Superconductivity and Magnetism in Lanthanide and Actinide Intermetallic Compounds*, Handbook on the Physics and Chemistry of Rare Earths, Vol. 34 (Elsevier, 2004) pp. 135 – 287.
 [7] C. Pfleiderer, Rev. Mod. Phys. **81**, 1551 (2009).
 [8] M. Sigrist and K. Ueda, Rev. Mod. Phys. **63**, 239 (1991).
 [9] K. H. Bennemann and J. B. Ketterson, eds., *Superconductivity Volume 1: Conventional and Unconventional Superconductors, Volume 2: Novel Superconductors* (Springer Berlin Heidelberg, 2008).
 [10] N. D. Mathur, F. M. Grosche, S. R. Julian, I. R. Walker, D. M. Freye, R. K. W. Haselwimmer, and G. G. Lonzarich, Nature **394**, 39 (1998).
 [11] T. Park, F. Ronning, H. Q. Yuan, M. B. Salamon, R. Movshovich, J. L. Sarrao, and J. D. Thompson, Nature **440**, 65 (2006).
 [12] P. Gegenwart, Q. Si, and F. Steglich, Nature Phys **4**, 186 (2008).
 [13] G. Knebel, D. Aoki, J.-P. Brison, and J. Flouquet, J. Phys. Soc. Jpn. **77**, 114704 (2008).
 [14] Y. Nakai, T. Iye, S. Kitagawa, K. Ishida, H. Ikeda, S. Kasahara, H. Shishido, T. Shibauchi, Y. Matsuda, and T. Terashima, Phys. Rev. Lett. **105** (2010), 10.1103/physrevlett.105.107003.
 [15] K. Hashimoto, K. Cho, T. Shibauchi, S. Kasa-

- hara, Y. Mizukami, R. Katsumata, Y. Tsuruhara, T. Terashima, H. Ikeda, M. A. Tanatar, H. Kitano, N. Salovich, R. W. Giannetta, P. Walmsley, A. Carrington, R. Prozorov, and Y. Matsuda, *Science* **336**, 1554 (2012).
- [16] T. Shibauchi, A. Carrington, and Y. Matsuda, *Annu. Rev. Condens. Matter Phys.* **5**, 113 (2014).
- [17] E. Pavarini, E. Koch, and P. Coleman, *Many-Body Physics: From Kondo to Hubbard Chapter 1, 1.1-1.34* (Forschungszentrum Jülich, 2015) arXiv:1509.05769 .
- [18] G. R. Stewart, *Rev. Mod. Phys.* **56**, 755 (1984).
- [19] R. Joynt and L. Taillefer, *Rev. Mod. Phys.* **74**, 235 (2002).
- [20] N. T. Huy, A. Gasparini, D. E. de Nijs, Y. Huang, J. C. P. Klaasse, T. Gortenmulder, A. de Visser, A. Hamann, T. Görlach, and H. v. Löhneysen, *Phys. Rev. Lett.* **99** (2007), 10.1103/physrevlett.99.067006.
- [21] D. Aoki, K. Ishida, and J. Flouquet, *J. Phys. Soc. Jpn.* **88**, 022001 (2019).
- [22] M. Tsujimoto, Y. Matsumoto, T. Tomita, A. Sakai, and S. Nakatsuji, *Phys. Rev. Lett.* **113** (2014), 10.1103/physrevlett.113.267001.
- [23] E. Bauer and J. Thompson, *Annu. Rev. Condens. Matter Phys.* **6**, 137 (2015).
- [24] J. D. Thompson and Z. Fisk, *J. Phys. Soc. Jpn.* **81**, 011002 (2012).
- [25] M. Kenzelmann, T. Strassle, C. Niedermayer, M. Sigrist, B. Padmanabhan, M. Zolliker, A. D. Bianchi, R. Movshovich, E. D. Bauer, J. L. Sarrao, and J. D. Thompson, *Science* **321**, 1652 (2008).
- [26] G. Knebel, D. Aoki, J.-P. Brison, L. Howald, G. Laperot, J. Panarin, S. Raymond, and J. Flouquet, *Phys. Status Solidi (b)* **247**, 557 (2010).
- [27] K. Izawa, H. Yamaguchi, Y. Matsuda, H. Shishido, R. Settai, and Y. Onuki, *Phys. Rev. Lett.* **87** (2001), 10.1103/physrevlett.87.057002.
- [28] C. Stock, C. Broholm, J. Hudis, H. J. Kang, and C. Petrovic, *Phys. Rev. Lett.* **100** (2008), 10.1103/physrevlett.100.087001.
- [29] K. An, T. Sakakibara, R. Settai, Y. Onuki, M. Hiragi, M. Ichioka, and K. Machida, *Phys. Rev. Lett.* **104** (2010), 10.1103/physrevlett.104.037002.
- [30] M. P. Allan, F. Massee, D. K. Morr, J. V. Dyke, A. W. Rost, A. P. Mackenzie, C. Petrovic, and J. C. Davis, *Nature Phys* **9**, 468 (2013).
- [31] B. B. Zhou, S. Misra, E. H. da Silva Neto, P. Aynajian, R. E. Baumbach, J. D. Thompson, E. D. Bauer, and A. Yazdani, *Nature Phys* **9**, 474 (2013).
- [32] V. A. Sidorov, M. Nicklas, P. G. Pagliuso, J. L. Sarrao, Y. Bang, A. V. Balatsky, and J. D. Thompson, *Phys. Rev. Lett.* **89** (2002), 10.1103/physrevlett.89.157004.
- [33] Y. Nakajima, H. Shishido, H. Nakai, T. Shibauchi, K. Behnia, K. Izawa, M. Hedo, Y. Uwatoko, T. Matsumoto, R. Settai, Y. Ōnuki, H. Kontani, and Y. Matsuda, *J. Phys. Soc. Jpn.* **76**, 024703 (2007).
- [34] W. Bao, P. G. Pagliuso, J. L. Sarrao, J. D. Thompson, Z. Fisk, J. W. Lynn, and R. W. Erwin, *Phys. Rev. B* **62**, R14621 (2000).
- [35] H. Hegger, C. Petrovic, E. G. Moshopoulou, M. F. Hundley, J. L. Sarrao, Z. Fisk, and J. D. Thompson, *Phys. Rev. Lett.* **84**, 4986 (2000).
- [36] H. Shishido, R. Settai, S. Araki, T. Ueda, Y. Inada, T. C. Kobayashi, T. Muramatsu, Y. Haga, and Y. Ōnuki, *Phys. Rev. B* **66** (2002), 10.1103/physrevb.66.214510.
- [37] T. Park, M. J. Graf, L. Boulaevskii, J. L. Sarrao, and J. D. Thompson, *Proceedings of the National Academy of Sciences* **105**, 6825 (2008).
- [38] H. Shishido, R. Settai, H. Harima, and Y. Ōnuki, *J. Phys. Soc. Jpn.* **74**, 1103 (2005).
- [39] Y. Ida, R. Settai, Y. Ota, F. Honda, and Y. Ōnuki, *J. Phys. Soc. Jpn.* **77**, 084708 (2008).
- [40] D. Huang and J. E. Hoffman, *Annu. Rev. Condens. Matter Phys.* **8**, 311 (2017).
- [41] D.-H. Lee, *Chinese Phys. B* **24**, 117405 (2015).
- [42] J. J. Lee, F. T. Schmitt, R. G. Moore, S. Johnston, Y.-T. Cui, W. Li, M. Yi, Z. K. Liu, M. Hashimoto, Y. Zhang, D. H. Lu, T. P. Devereaux, D.-H. Lee, and Z.-X. Shen, *Nature* **515**, 245 (2014).
- [43] L. Rademaker, Y. Wang, T. Berlijn, and S. Johnston, *New J. Phys.* **18**, 022001 (2016).
- [44] Y. Mizukami, H. Shishido, T. Shibauchi, M. Shimozawa, S. Yasumoto, D. Watanabe, M. Yamashita, H. Ikeda, T. Terashima, H. Kontani, and Y. Matsuda, *Nature Phys* **7**, 849 (2011).
- [45] S. K. Goh, Y. Mizukami, H. Shishido, D. Watanabe, S. Yasumoto, M. Shimozawa, M. Yamashita, T. Terashima, Y. Yanase, T. Shibauchi, A. I. Buzdin, and Y. Matsuda, *Phys. Rev. Lett.* **109** (2012), 10.1103/physrevlett.109.157006.
- [46] M. Shimozawa, S. Goh, R. Endo, R. Kobayashi, T. Watashige, Y. Mizukami, H. Ikeda, H. Shishido, Y. Yanase, T. Terashima, T. Shibauchi, and Y. Matsuda, *Phys. Rev. Lett.* **112** (2014), 10.1103/physrevlett.112.156404.
- [47] T. Yamanaka, M. Shimozawa, R. Endo, Y. Mizukami, H. Shishido, T. Terashima, T. Shibauchi, Y. Matsuda, and K. Ishida, *Phys. Rev. B* **92** (2015), 10.1103/physrevb.92.241105.
- [48] M. Naritsuka, P. Rosa, Y. Luo, Y. Kasahara, Y. Tokiwa, T. Ishii, S. Miyake, T. Terashima, T. Shibauchi, F. Ronning, J. Thompson, and Y. Matsuda, *Phys. Rev. Lett.* **120** (2018), 10.1103/physrevlett.120.187002.
- [49] M. Naritsuka, S. Nakamura, Y. Kasahara, T. Terashima, R. Peters, and Y. Matsuda, *Phys. Rev. B* **100** (2019), 10.1103/physrevb.100.024507.
- [50] H. Shishido, T. Shibauchi, K. Yasu, T. Kato, H. Kontani, T. Terashima, and Y. Matsuda, *Science* **327**, 980 (2010).
- [51] M. Shimozawa, S. K. Goh, T. Shibauchi, and Y. Matsuda, *Rep. Prog. Phys.* **79**, 074503 (2016).
- [52] C. Petrovic, P. G. Pagliuso, M. F. Hundley, R. Movshovich, J. L. Sarrao, J. D. Thompson, Z. Fisk, and P. Monthoux, *J. Phys.: Condens. Matter* **13**, L337 (2001).
- [53] R. Settai, T. Takeuchi, and Y. Ōnuki, *J. Phys. Soc. Jpn.* **76**, 051003 (2007).
- [54] Y. Kawasaki, S. Kawasaki, M. Yashima, T. Mito, G. qing Zheng, Y. Kitaoka, H. Shishido, R. Settai, Y. Haga, and Y. Ōnuki, *J. Phys. Soc. Jpn.* **72**, 2308 (2003).
- [55] H. Sakai, S. E. Brown, S.-H. Baek, F. Ronning, E. D. Bauer, and J. D. Thompson, *Phys. Rev. Lett.* **107** (2011), 10.1103/physrevlett.107.137001.
- [56] S. Ikeda, H. Shishido, M. Nakashima, R. Settai, D. Aoki, Y. Haga, H. Harima, Y. Aoki, T. Namiki, H. Sato, and Y. Ōnuki, *J. Phys. Soc. Jpn.* **70**, 2248 (2001).
- [57] G. Knebel, M.-A. Méasson, B. Salce, D. Aoki,

- D. Braithwaite, J. P. Brison, and J. Flouquet, *J. Phys.: Condens. Matter* **16**, 8905 (2004).
- [58] Y. Nakajima, K. Izawa, Y. Matsuda, S. Uji, T. Terashima, H. Shishido, R. Settai, Y. Onuki, and H. Kontani, *J. Phys. Soc. Jpn.* **73**, 5 (2004).
- [59] S. Raymond and G. Lapertot, *Phys. Rev. Lett.* **115** (2015), 10.1103/physrevlett.115.037001.
- [60] A. Bianchi, R. Movshovich, N. Oeschler, P. Gegenwart, F. Steglich, J. D. Thompson, P. G. Pagliuso, and J. L. Sarrao, *Phys. Rev. Lett.* **89** (2002), 10.1103/physrevlett.89.137002.
- [61] A. M. Clogston, *Phys. Rev. Lett.* **9**, 266 (1962).
- [62] Y. Matsuda and H. Shimahara, *J. Phys. Soc. Jpn.* **76**, 051005 (2007).
- [63] A. Bianchi, R. Movshovich, C. Capan, P. G. Pagliuso, and J. L. Sarrao, *Phys. Rev. Lett.* **91** (2003), 10.1103/physrevlett.91.187004.
- [64] K. Kumagai, M. Saitoh, T. Oyaizu, Y. Furukawa, S. Takashima, M. Nohara, H. Takagi, and Y. Matsuda, *Phys. Rev. Lett.* **97** (2006), 10.1103/physrevlett.97.227002.
- [65] Y. Hatakeyama and R. Ikeda, *Phys. Rev. B* **83** (2011), 10.1103/physrevb.83.224518.
- [66] K. Kumagai, H. Shishido, T. Shibauchi, and Y. Matsuda, *Phys. Rev. Lett.* **106** (2011), 10.1103/physrevlett.106.137004.
- [67] S.-Z. Lin, D. Y. Kim, E. D. Bauer, F. Ronning, J. Thompson, and R. Movshovich, *Phys. Rev. Lett.* **124** (2020), 10.1103/physrevlett.124.217001.
- [68] J. L. Sarrao and J. D. Thompson, *J. Phys. Soc. Jpn.* **76**, 051013 (2007).
- [69] G. Sparn, R. Borth, E. Lengyel, P. Pagliuso, J. Sarrao, F. Steglich, and J. Thompson, *Physica B: Condensed Matter* **319**, 262 (2002).
- [70] M. Yashima, H. Mukuda, Y. Kitaoka, H. Shishido, R. Settai, and Y. Onuki, *Phys. Rev. B* **79** (2009), 10.1103/physrevb.79.214528.
- [71] G. Knebel, D. Aoki, D. Braithwaite, B. Salce, and J. Flouquet, *Phys. Rev. B* **74** (2006), 10.1103/physrevb.74.020501.
- [72] A. Benoit, J. Boucherle, P. Convert, J. Flouquet, J. Palteau, and J. Schweizer, *Solid State Communications* **34**, 293 (1980).
- [73] J. M. Lawrence and S. M. Shapiro, *Phys. Rev. B* **22**, 4379 (1980).
- [74] G. Knebel, D. Braithwaite, P. C. Canfield, G. Lapertot, and J. Flouquet, *Phys. Rev. B* **65** (2001), 10.1103/physrevb.65.024425.
- [75] T. Moriya and K. Ueda, *Advances in Physics* **49**, 555 (2000).
- [76] V. I. Zaremba, U. C. Rodewald, R.-D. Hoffmann, Y. M. Kalychak, and R. Pöttgen, *Z. anorg. allg. Chem.* **629**, 1157 (2003).
- [77] H. T. Huy, S. Noguchi, N. V. Hieu, X. Shao, T. Sugimoto, and T. Ishida, *Journal of Magnetism and Magnetic Materials* **321**, 2425 (2009).
- [78] Y. Uwatoko, M. Hedo, N. Kurita, M. Koeda, M. Abliz, and T. Matsumoto, *Physica B: Condensed Matter* **329-333**, 1658 (2003), proceedings of the 23rd International Conference on Low Temperature Physics.
- [79] R. Peters, Y. Tada, and N. Kawakami, *Phys. Rev. B* **88** (2013), 10.1103/physrevb.88.155134.
- [80] J.-H. She and A. V. Balatsky, *Phys. Rev. Lett.* **109** (2012), 10.1103/physrevlett.109.077002.
- [81] T. Schneider and A. Schmidt, *Phys. Rev. B* **47**, 5915 (1993).
- [82] M. Tinkham, *Introduction to Superconductivity, 2nd ed.* (McGraw-Hill, 1996).
- [83] M. Tinkham, *Phys. Rev.* **129**, 2413 (1963).
- [84] N. R. Werthamer, E. Helfand, and P. C. Hohenberg, *Phys. Rev.* **147**, 295 (1966).
- [85] S. Fujimoto, *J. Phys. Soc. Jpn.* **76**, 051008 (2007).
- [86] D. Maruyama, M. Sigrist, and Y. Yanase, *J. Phys. Soc. Jpn.* **81**, 034702 (2012).
- [87] E. Bauer and M. Sigrist, eds., *Non-Centrosymmetric Superconductors* (Springer Berlin Heidelberg, 2012).
- [88] E. I. Rashba, *Sov. Phys. Solid State* **2**, 1109 (1960).
- [89] Y. A. Bychkov and E. I. Rasha, *JETP Lett.* **39**, 78 (1984).
- [90] T. Ishii, R. Toda, Y. Hanaoka, Y. Tokiwa, M. Shimozawa, Y. Kasahara, R. Endo, T. Terashima, A. Nevidomskyy, T. Shibauchi, and Y. Matsuda, *Phys. Rev. Lett.* **116** (2016), 10.1103/physrevlett.116.206401.
- [91] M. Naritsuka, T. Ishii, S. Miyake, Y. Tokiwa, R. Toda, M. Shimozawa, T. Terashima, T. Shibauchi, Y. Matsuda, and Y. Kasahara, *Phys. Rev. B* **96** (2017), 10.1103/physrevb.96.174512.
- [92] R. P. Kaur, D. F. Agterberg, and M. Sigrist, *Phys. Rev. Lett.* **94** (2005), 10.1103/physrevlett.94.137002.
- [93] T. Yoshida, M. Sigrist, and Y. Yanase, *Phys. Rev. B* **86** (2012), 10.1103/physrevb.86.134514.
- [94] T. Yoshida, M. Sigrist, and Y. Yanase, *J. Phys. Soc. Jpn.* **82**, 074714 (2013).
- [95] T. Yoshida, M. Sigrist, and Y. Yanase, *Phys. Rev. Lett.* **115** (2015), 10.1103/physrevlett.115.027001.
- [96] T. Watanabe, T. Yoshida, and Y. Yanase, *Phys. Rev. B* **92** (2015), 10.1103/physrevb.92.174502.
- [97] T. Yoshida, A. Daido, Y. Yanase, and N. Kawakami, *Phys. Rev. Lett.* **118** (2017), 10.1103/physrevlett.118.147001.
- [98] A. Daido and Y. Yanase, *Phys. Rev. B* **94** (2016), 10.1103/physrevb.94.054519.
- [99] A. Daido and Y. Yanase, *Phys. Rev. B* **95** (2017), 10.1103/physrevb.95.134507.
- [100] M. Sato and S. Fujimoto, *Phys. Rev. B* **79** (2009), 10.1103/physrevb.79.094504.
- [101] M. Sato and S. Fujimoto, *Phys. Rev. Lett.* **105** (2010), 10.1103/physrevlett.105.217001.
- [102] T. Park, E. D. Bauer, and J. D. Thompson, *Phys. Rev. Lett.* **101** (2008), 10.1103/physrevlett.101.177002.
- [103] T. Yamanaka, M. Shimozawa, H. Shishido, S. Kitagawa, H. Ikeda, T. Shibauchi, T. Terashima, Y. Matsuda, and K. Ishida, *Phys. Rev. B* **96** (2017), 10.1103/physrevb.96.060507.
- [104] G. Nakamine, T. Yamanaka, S. Kitagawa, M. Naritsuka, T. Ishii, T. Shibauchi, T. Terashima, Y. Kasahara, Y. Matsuda, and K. Ishida, *Phys. Rev. B* **99** (2019), 10.1103/physrevb.99.081115.
- [105] T. Tayama, A. Harita, T. Sakakibara, Y. Haga, H. Shishido, R. Settai, and Y. Onuki, *Phys. Rev. B* **65** (2002), 10.1103/physrevb.65.180504.
- [106] B. J. Ramshaw, S. E. Sebastian, R. D. McDonald, J. Day, B. S. Tan, Z. Zhu, J. B. Betts, R. Liang, D. A. Bonn, W. N. Hardy, and N. Harrison, *Science* **348**, 317 (2015).
- [107] T. Ebihara, I. Umehara, A. Albessard, K. Satoh, and Y. Onuki, *Physica B: Condensed Matter* **186-188**, 123 (1993).

- [108] N. Harrison, U. Alver, R. G. Goodrich, I. Vekhter, J. L. Sarrao, P. G. Pagliuso, N. O. Moreno, L. Balicas, Z. Fisk, D. Hall, R. T. Macaluso, and J. Y. Chan, *Phys. Rev. Lett.* **93** (2004), 10.1103/physrevlett.93.186405.
- [109] N. Oeschler, P. Gegenwart, M. Lang, R. Movshovich, J. L. Sarrao, J. D. Thompson, and F. Steglich, *Phys. Rev. Lett.* **91** (2003), 10.1103/physrevlett.91.076402.
- [110] S. Raymond, G. Knebel, D. Aoki, and J. Flouquet, *Phys. Rev. B* **77** (2008), 10.1103/physrevb.77.172502.
- [111] L. D. Pham, T. Park, S. Maquilon, J. D. Thompson, and Z. Fisk, *Phys. Rev. Lett.* **97** (2006), 10.1103/physrevlett.97.056404.
- [112] M. Nicklas, O. Stockert, T. Park, K. Habicht, K. Kiefer, L. D. Pham, J. D. Thompson, Z. Fisk, and F. Steglich, *Phys. Rev. B* **76** (2007), 10.1103/physrevb.76.052401.
- [113] C. H. Booth, E. D. Bauer, A. D. Bianchi, F. Ronning, J. D. Thompson, J. L. Sarrao, J. Y. Cho, J. Y. Chan, C. Capan, and Z. Fisk, *Phys. Rev. B* **79** (2009), 10.1103/physrevb.79.144519.
- [114] Y. Michishita and R. Peters, *Phys. Rev. B* **99** (2019), 10.1103/physrevb.99.155141.
- [115] K. Nogaki and Y. Yanase, *Phys. Rev. B* **102** (2020), 10.1103/physrevb.102.165114.
- [116] S. Wolf and S. Rachel, *Phys. Rev. B* **102** (2020), 10.1103/physrevb.102.174512.
- [117] E. Bauer, G. Hilscher, H. Michor, C. Paul, E. W. Scheidt, A. Griбанov, Y. Seropegin, H. Noël, M. Sigrist, and P. Rogl, *Phys. Rev. Lett.* **92** (2004), 10.1103/physrevlett.92.027003.
- [118] N. Kimura, Y. Muro, and H. Aoki, *J. Phys. Soc. Jpn.* **76**, 051010 (2007).
- [119] Y. Okuda, Y. Miyauchi, Y. Ida, Y. Takeda, C. Tonohiro, Y. Oduchi, T. Yamada, N. D. Dung, T. D. Matsuda, Y. Haga, T. Takeuchi, M. Hagiwara, K. Kindo, H. Harima, K. Sugiyama, R. Settai, and Y. Ōnuki, *J. Phys. Soc. Jpn.* **76**, 044708 (2007).
- [120] S. Khim, J. F. Landaeta, J. Banda, N. Banner, M. Brando, P. M. R. Brydon, D. Hafner, R. K uchler, R. Cardoso-Gil, U. Stockert, A. P. Mackenzie, D. F. Agterberg, C. Geibel, and E. Hassinger, arxiv:2101.09522 (2021).
- [121] M. Shahzad and P. Sengupta, *J. Phys.: Condens. Matter* **29**, 305802 (2017).
- [122] S. Okumura, Y. Kato, and Y. Motome, *Physica B: Condensed Matter* **536**, 223 (2018).
- [123] N. F. Yuan, C. L. Wong, and K. Law, *Physica E: Low-dimensional Systems and Nanostructures* **55**, 30 (2014).
- [124] N. Read and D. Green, *Phys. Rev. B* **61**, 10267 (2000).